CHALMERS
UNIVERSITY OF TECHNOLOGY

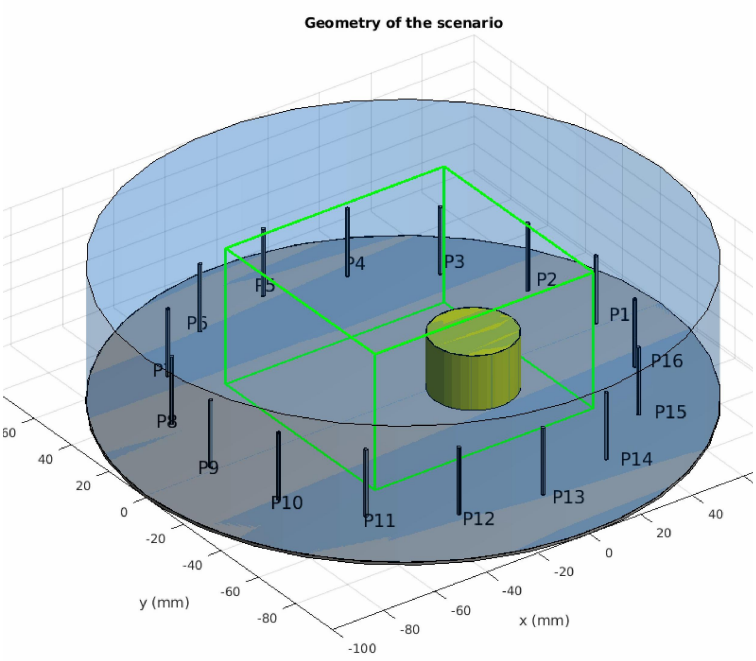

Regularized algorithms for applications in microwave thermometry

Optimizing the regularization parameter for an inverse and ill-posed problem using Tikhonov's regularization methods

Master's thesis in Engineering Mathematics and Computational Science

Rani Alsaberi

DEPARTMENT OF MATHEMATICAL SCIENCES
CHALMERS UNIVERSITY OF TECHNOLOGY
Gothenburg, Sweden 2024
www.chalmers.se

Master's thesis 2024

Regularized algorithms for applications in microwave thermometry

Optimizing the regularization parameter for an inverse and ill-posed problem using Tikhonov's regularization methods

RANI ALSABERI

CHALMERS
UNIVERSITY OF TECHNOLOGY

Department of Mathematical Sciences
Chalmers University of Technology
Gothenburg, Sweden 2024

Regularized algorithms for applications in microwave thermometry
Optimizing the regularization parameter for an inverse and ill-posed problem using Tikhonov's regularization methods

© RANI ALSABERI, 2024.

Supervisor: Larisa Beilina, Department of Mathematical Sciences
Examiner: Larisa Beilina, Department of Mathematical Sciences

Master's Thesis 2024
Department of Mathematical Sciences
Chalmers University of Technology
SE-412 96 Gothenburg

Abstract

This study explores the optimization of the regularization parameter for Tikhonov's functional, which is derived from the vector wave equation, a partial differential equation (PDE), and transformed into a volume integral equation. Solving this equation using Tikhonov's functionals provides three different approaches, each with varying numbers of regularization parameters. To identify the optimal regularization parameters, three methods were employed: the L-curve method, the fixed point algorithm, and Morozov's discrepancy principle.

The L-curve method and the fixed point algorithm both indicated that a regularization parameter of 1 is optimal, yielding acceptable results across various reconstruction scenarios. However, Morozov's discrepancy principle consistently produced superior results, albeit with a significant dependency on the initial reconstruction matrix. Ultimately, while Morozov's discrepancy principle shows the most promise for optimizing Tikhonov's functional, it is not yet viable for practical use without further refinement. Moreover, compared to previous studies with a similar setup, this study employs the finite difference method, unlike past works where the finite element method was employed.

The code can be found at the link given in [28].

Keywords: Tikhonov's functional, regularization parameter, L-curve method, fixed point algorithm, Morozov's discrepancy principle, hyperthermia, ill-posed problem.

Acknowledgements

I would like to express my sincere gratitude to my supervisor, Larisa Beilina, for their guidance and support throughout my master's thesis journey. Their insightful feedback has been instrumental in shaping this work. So for that, thank you Larisa!

Outside the realm of this thesis, I extend my heartfelt thanks to Chalmers Tekniska Högskola and its professors for mentoring me in mathematical engineering. Their input has greatly contributed to my academic growth.

I would also like to express my special appreciation to my friends and family for their endless love and support throughout my academic life, and life in general.

Rani Alsaberi, Gothenburg, May 2024

Contents

List of Figures

List of Tables

1

Introduction

Cancer is one of the leading causes of death globally, causing nearly 10 million deaths in 2019. This accounts for one in six deaths worldwide [31]. According to the National Cancer Institution, cancer is a disease characterized by uncontrolled cell growth and the potential to spread to other parts of the body. It can originate almost anywhere in the human body, which is composed of trillions of cells. Under normal circumstances old cells are replaced in an orderly manner. However, this process can malfunction, leading to the formation of damaged cells that may form tumors [34].

Chemotherapy is a widely recognized method for treating cancer. It is considered a systemic treatment because the drugs travel throughout the body, which allows them to target and kill cancerous cells. In addition to chemotherapy, there are other treatments such as radiation therapy. It uses targeted radiation to kill or damage cancer cells in a particular area. Meaning these local treatments only affect one part of the body.

Microwave hyperthermia/thermometry tumor therapy is another method used to treat cancer. It is in fact, one of the oldest methods [15], and has enhanced the effectiveness of conventional cancer treatments such as chemotherapy and radiotherapy [30]. Hyperthermia works by heating cancerous tissues using electromagnetic waves, raising the temperature of the cells to a level higher than normal, to about 40-44 degrees centigrade [4]. This selective heating aims to target only the cancerous cells while sparing the surrounding healthy tissues [36]. To ensure precision and real-time feedback during treatment, the integration of a reliable temperature monitoring system is essential [7].

Over the past few decades, in addition to microwave thermometry, numerous methods have been proposed in the literature. Among them are invasive measurements at specific tumor-related reference points [9, 26], and MR-guided (magnetic resonance) thermometry [12, 18, 35], both of which are currently employed in clinical settings. While the use of inexpensive and easily accessible multipoint thermal probes equipped with thermocouples, thermistors, or fiber optic sensors remains a widely accepted standard, the invasive nature of this procedure restricts temperature data to a limited number of monitoring positions. On the other hand, MR-guided thermometry offers non-invasive, three-dimensional temperature monitoring. However, its real-time acquisition speed currently falls short [35]. Moreover, MR systems tend to be expensive and non-compatible with other systems. Additionally, MR technol-

ogy is unsuitable for intraoperative monitoring in patients with MR-incompatible pacemakers or artificial heart valves [11].

Given these considerations, microwave thermometry becomes an attractive method, offering insights in three dimensions while utilizing the same antennas for heating [23]. It addresses both the cost and information (the thermal profiles) constraints effectively.

In this study, we will adopt a framework similar to that used in [3, 4, 5]. Specifically, our investigation focuses on a cylindrical scenario involving an annular phased array system comprising 16 monopole antennas designed to operate within the ISM band (industrial, scientific, and medical band) of 915 MHz. This frequency band is chosen because it offers an optimal balance between the penetration depth of electromagnetic waves into biological tissues and imaging resolution. Additionally, the dielectric changes resulting from temperature variations at this frequency are significant enough to be detected through microwave imaging techniques. The 16 antennas are immersed in a coupling fluid consisting of a 20:7 mixture of isopropyl alcohol to water, chosen based on [3] to balance conductive loss, relative permittivity, and antenna matching. We refer to the problem at hand as the dielectric problem. The aim is to optimize a dielectric function such that the heat is targeted optimally, meaning only the cancerous cells are heated and destroyed without affecting the surrounding healthy tissues.

A depiction of the dielectric problem and the return loss of the scattered parameters (S_{11}) of the designed antenna for the frequency band 915 MHz, are seen in Figures 1.1 and 1.2 respectively [3]. The dotted horizontal red line in Figure 1.2 indicates where valuable information is obtained, as any data below -10 dB is not considered valuable.

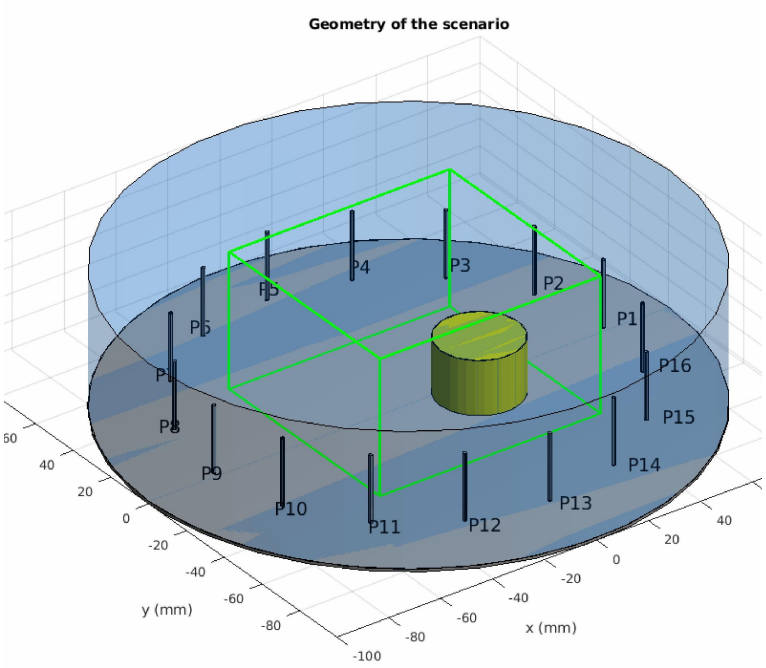

Figure 1.1: The dielectric problem with the 16 monopole antennas immersed in a liquid tank. The region of interest is highlighted in green.

To accurately model the microwave hyperthermia and predict the thermal distribution within the tissue, we begin with a partial differential equation, i.e. the vector wave equation, that describes how heat transfer and electromagnetic waves propagate [13, 29], which is transformed to a volume integral equation (VIE). Various mathematical and analytical methods have been applied to investigate three-dimensional vector electromagnetic problems related to volume integral equations, as presented in previous studies [14]. Methods applied in computational electromagnetics with the dielectric problem, are documented in the literature [3, 4, 5].

In our study and many others, the considered volume integral equation (VIE) is a Fredholm integral equation of the first kind [19]. Due to its ill-posed nature, we formulate the solution of the VIE as an optimal control problem aimed at minimizing Tikhonov's regularization functional [24], transforming it into a linear (regularized) least squares problem. This procedure allows us to explore different methods for reconstructing the dielectric problem, see Section 2. Unlike previous studies on the dielectric problem [3, 4, 5], that employed variations of the finite element method (FEM), our study utilizes a finite difference method (FDM) approach. This is our main objective in this study, comparing the FEM to the FDM. Furthermore, the reconstructions involve regularization parameters that need to be optimized, and we present three methods for this optimization in Section 2. The obtained results are presented in Section 3 and discussed in Section 4.

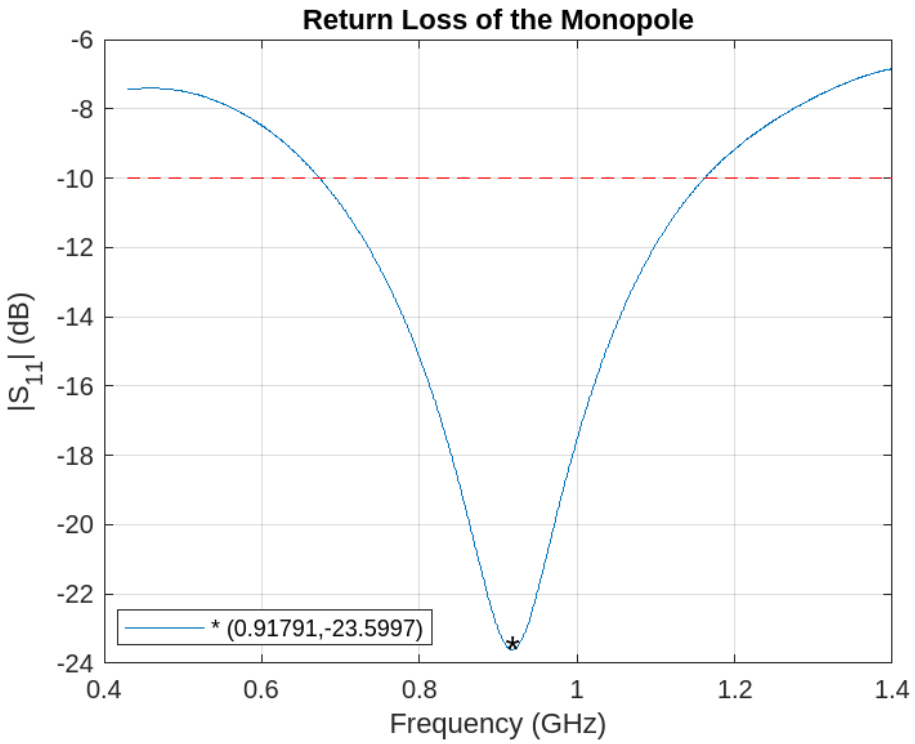

Figure 1.2: The return loss of the scattered parameter (S_{11}) of the designed antenna for the frequency band 915 MHz. The dotted horizontal red line indicates where valuable information is obtained, as any data below -10 dB is not considered valuable.

2

Theoretical Background and Methodology

The theoretical section is split into two primary parts. The first segment covers the prerequisites, providing the necessary mathematical background. While the second segment is the problem description, where we mathematically describe the dielectric problem, and the methods and algorithms employed.

2.1 Prerequisites

This segment primarily focuses on describing the different vector spaces utilized, but also stating and proving the singular value decomposition through the spectral theorem.

2.1.1 L^p and Hilbert space

In functional analysis, vector spaces play an integral role, especially function spaces, particularly when defining and investigating functions. Using a functional analytic approach, one considers a set of functions, where each function represents a point in the set. From there, one can explore the geometric and algebraic structures of the set. Such a space is named a *function space*. A mapping from one function space to another is referred to as an *operator*. A function defined on a function space is known as a *functional* [2].

There are many function spaces, including the space of continuous functions, the space of smooth functions, Sobolev spaces, Hölder spaces, and numerous others. However, we focus on defining the L^p-space and the Hilbert space. Let $(\Omega, \mathcal{F}, x)$ denote a σ-finite measure space, where Ω denotes the underlying space, $\mathcal{F}$ is the σ-algebra of measurable sets, and x is the measure [33].

Definition 2.1.1 (L_p-space)**.** The L_p-space, also known as the space of *Lebesgue integrable* functions on an open set $\Omega \subset \mathbb{R}^n$, denoted by $L_p(\Omega, \mathcal{F}, x)$ or for simplicity $L_p(\Omega)$. For $p \geq 1$ and $u \in L_p(\Omega)$, the space $L_p(\Omega)$ is defined as [32]:

$$L_p(\Omega) := \left\{ u : \Omega \to \mathbb{R}; \left(\int_\Omega |u(x)|^p dx \right)^{1/p} < \infty \right\}, \quad 1 \leq p < \infty. \tag{2.1}$$

In particular, the L_2-space will be used. For ease of writing, the L_2-norm is denoted as : $\|\cdot\|_2$ or simply $\|\cdot\|$.

Moreover, the Hilbert space H^k is defined as [17]:
Definition 2.1.2 (H^k-space)**.**

$$H^k(\Omega, \mathcal{F}, x) = H^k(\Omega) := \{u \in L_2(\Omega) : \frac{\partial u}{\partial x_j} \in L_2(\Omega), \quad j = 1, \ldots, n, \quad \text{and} \\ \frac{\partial^2 u}{\partial x_{j_1} \partial x_{j_2}} \in L_2(\Omega), \quad j_1, j_2 = 1, \ldots, n, \quad \text{and} \quad \ldots \\ \text{and} \quad \frac{\partial^k u}{\partial x_{j_1} \partial x_{j_2} \ldots \partial x_{j_k}} \in L_2(\Omega), \quad j_1, j_2, \ldots, j_k = 1, \ldots, n\} \tag{2.2}$$

In particular, the H^1-space will be used, i.e

$$H^1(\Omega) := \left\{ u \in L_2(\Omega) : \frac{\partial u}{\partial x_j} \in L_2(\Omega), \quad j = 1, \ldots, n \right\}. \tag{2.3}$$

2.1.2 The Spectral Theorem and SVD

The Singular Value Decomposition (SVD), is useful when it comes to solving ill-conditioned problems, i.e rank deficient problems. However, the spectral theorem needs to be proven first . We'll start with a lemma:
Lemma 2.1.1. *For a real symmetric $n \times n$ matrix A, all of it's eigenvalues are real [8].*

Proof. Let $\lambda \in \mathbb{C}$ be an eigenvalue of A with corresponding eigenvector $v \in \mathbb{C}^n$

$$\begin{aligned} (Av)^T \overline{v} &= v^T A^T \overline{v} \\ &= v^T (A\overline{v}) \\ &= v^T \left(\overline{A}\overline{v}\right) \\ &= v^T \left(\overline{Av}\right) \\ &= v^T \left(\overline{\lambda v}\right) \\ &= \overline{\lambda} v^T \overline{v} \end{aligned}$$

$$(Av)^T \overline{v} = \lambda v^T \overline{v}.$$

■

Comparing the last two lines it's evident that $\bar{\lambda} = \lambda$ that is, $\lambda \in \mathbb{R}$.

It's rather trivial that for an arbitrary matrix A, that $A^T A$ is symmetric. Moreover, it's positive semidefinite since $A^T A\bar{v} = \lambda\bar{v}$, multiplying by $\bar{v}^T$ from the left and solving for lambda gives, $\lambda = \frac{\bar{v}^T A^T A \bar{v}}{\bar{v}^T \bar{v}} = \frac{\|A\bar{v}\|_2^2}{\|\bar{v}\|_2^2} \geq 0$.

Theorem 2.1.2. *Let M be an $n \times n$ symmetric matrix, then there exists an orthogonal matrix R such that $R^T MR$ is diagonal. That is, any symmetric matrix is diagonalizable [8].*

Proof by induction. **Base case:**
M and $\bar{v}$ both are scalars, meaning $M\bar{v} = \lambda\bar{v} \implies M = \lambda$. Therefore, any non-zero real scalar $\bar{v}$ will form a basis.

The induction hypothesis:
Every $k \times k$ symmetric matrix is diagonalizable for $k = 1, \ldots, n-1$.

Choose an eigenvalue $\lambda_1 \in \mathbb{R}$, by Lemma 2.2.1. Moreover, normalize the corresponding eigenvector, i.e $|\bar{v_1}| = 1$. Now using the Gram-Schmidt algorithm (see for example [6] for details), an orthonormal basis $B = \bar{v_1}, \bar{v_2}, \ldots, \bar{v_n}$ can be obtained for $\mathbb{R}^n$.

Define $Q = [\bar{v_1}, \bar{v_2}, \ldots, \bar{v_n}]$. The columns of Q are orthonormal and hence Q is an orthogonal matrix. Define $A = Q^T MQ$, then

$$A^T = \left(Q^T MQ\right)^T = Q^T M^T Q = Q^T MQ = A,$$

therefore A is symmetric. In block matrix form, by multiplying the standard basis vector $\mathbf{e}_1$, from the right, A becomes

$$Q^T MQ\mathbf{e}_1 = Q^T M\bar{v_1} = \lambda_1 Q^T \bar{v_1} = \lambda_1 \begin{bmatrix} 1 \\ 0 \\ \vdots \\ 0 \end{bmatrix}.$$

So, A has the matrix block form

$$\begin{bmatrix} \lambda_1 & 0 \\ 0 & C \end{bmatrix},$$

where C is of size $(n-1 \times n-1)$ and symmetric.

Now by the induction hypothesis, there exists a diagonal matrix D and orthogonal matrix Q such that $D = Q^{-1}CQ = Q^T CQ$. Define

$$R = P \begin{bmatrix} 1 & 0 \\ 0 & Q \end{bmatrix}.$$

Now we'll show that R is orthogonal and $R^T MR$ is diagonal. For the first part,

$$R^{-1} = \begin{bmatrix} 1 & 0 \\ 0 & Q^{-1} \end{bmatrix} P^{-1} = \begin{bmatrix} 1 & 0 \\ 0 & Q^T \end{bmatrix} P^T = R^T.$$

For the second part,

$$R^T MR = \begin{bmatrix} 1 & 0 \\ 0 & Q^T \end{bmatrix} P^T MP \begin{bmatrix} 1 & 0 \\ 0 & Q \end{bmatrix} = \begin{bmatrix} \lambda_1 & 0 \\ 0 & D \end{bmatrix}.$$

In conclusion, we can say that there exists an orthogonal matrix R such that $R^T MR$ is diagonal. That is, there exists an orthonormal basis for $\mathbb{R}^n$ consisting of eigenvalues of M.

■

Now that we've proved the spectral theorem we are ready to prove the SVD theorem.

Theorem 2.1.3. *Let A be an $m \times n$ matrix, then there exists a decomposition*

$$A = U\Sigma V^T$$

where U is an $m \times m$ orthogonal matrix, V is an $n \times n$ orthogonal matrix, and Σ is a diagonal $m \times n$ matrix, with entries $\sigma_1 \geq \sigma_2 \geq \cdots \geq \sigma_n$, where the σ's are the singular values [27].

Proof. As previously showed $A^T A$ is symmetric and positive semidefinite. Let $\lambda_1 > \cdots > \lambda_n \geq 0$ be its eigenvalues. Define the singular values as $\sigma_i = \sqrt{\lambda_i}$, and let D be the $n \times n$ diagonal matrix with diagonal entries $\sigma_1, \cdots, \sigma_n$. The spectral theorem gives a factorization

$$A^T A = VDV^T = \sum_{i=1}^{n} (\sigma_i)^2 \bar{v}_i \bar{v}_i^T$$

where V is an orthogonal $n \times n$ matrix. Note that $\ker\left(A^T A\right) = \ker(A)$. Since $A^T A$ is diagonalizable, by the spectral theorem, meaning there are exactly r non-zero eigenvalues, where $r = \operatorname{rank}(A)$. Now construct the unit eigenvector of $A^T A$, that is

$$\bar{u}_i = \frac{A\bar{v}_i}{\sigma_i}.$$

Now we realize that the i-th coloumn of $\bar{v}_i$ is V. Moreover let U be an $m \times m$ matrix where its i-th column is $\bar{u}_i$. Lastly, let Σ be a diagonal matrix whose i-th element is σ. Meaning in matrix form we obtain:

$$U = AV\Sigma^{-1} \implies A = U\Sigma V^T.$$

■

As previously mentioned the singular value decomposition is useful when the problem at hand does not have a full column rank. This means the solution to the least square problem that is, $\min_x \|Ax - b\|_2^2$, is not unique. The SVD for a rank-deficient matrix A looks as follows:

$$(U_1, U_2) \begin{pmatrix} \Sigma_1 & 0 \\ 0 & 0 \end{pmatrix} (V_1, V_2)^T = U_1 \Sigma_1 V_1^T \tag{2.4}$$

Where Σ_1 has size $r \times r$ and is non-singular, U_1 and V_1 have r columns and $r = rank(A)$.

Theorem 2.1.4. *Let $A{=}U_1\Sigma_1V_1^T$ be the rank-deficient SVD, then the solution of the the least squares problem [6]*

$$\min_x \|Ax-b\|_2^2$$

is $x{=}U_1\Sigma_1V_1^Tb$.

Proof. We have $\|Ax-b\|_2^2 = \left\|U_1\Sigma_1V_1^Tx-b\right\|_2^2$, and since Σ_1 has full rank it's also invertible. Let us construct the matrix $(U_1,\tilde{U_1})$, which by the definition square and orthogonal. Hence we have,

$$\begin{aligned}\left\|U_1\Sigma_1V_1^Tx-b\right\|_2^2 &= \left\|\begin{pmatrix}U_1^T\\ \tilde{U_1}^T\end{pmatrix}\left(U_1\Sigma_1V_1^Tx-b\right)\right\|_2^2\\ &= \left\|\begin{pmatrix}\Sigma_1V_1^Tx-U_1^Tb\\ -\tilde{U_1}^Tb\end{pmatrix}\right\|_2^2\\ &= \left\|\Sigma_1V_1^Tx-U_1^Tb\right\|_2^2+\left\|\tilde{U_1}^Tb\right\|_2^2.\end{aligned}$$

By making the first term zero, $\Sigma_1V_1^Tx = U_1^Tb$, one finds that the minimum of the least squares problem is given by $x = V_1\Sigma_1^{-1}U_1^Tb = A^+b$, where the matrix A^+ is called the Moore–Penrose inverse. ■

2.2 Problem description

In this segment the mathematics behind the employed model is explained. Arriving at three different ways of reconstructing the cylindrical scenario. Moreover, three methods are presented to optimize the regularization parameters.

2.2.1 Vector wave equation with the Silver-Müller radiation condition at infinity

To mathematically describe the problem at hand, i.e. the dielectric problem, we utilize the classic vector wave equation, as derived in [13], along with the Silver-Müller radiation condition at infinity,

$$\lim_{\rho\to\infty}\rho\left(\left(\nabla\times\widehat{E}_{sca}\right)\times\hat{x}-ik\widehat{E}_{sca}\right), \tag{2.5}$$

where $\rho=|x|$, as demonstrated in [29]. Combining these two elements yields,

$$\nabla\times\nabla\times\widehat{E}(r)-\omega^2\left(\frac{\varepsilon_r(r)}{c^2}+i\mu_0\frac{\sigma(r)}{\omega}\right)\widehat{E}(r)=i\omega\mu_0\widehat{J}(r),\quad r\in\mathbb{R}^3. \tag{2.6}$$

Here, $r=(x,y,z)$ represents the classic Cartesian coordinates,
$\widehat{E}(r)=\left(\widehat{E}_x(r),\widehat{E}_y(r),\widehat{E}_z,(r)\right)$, note that the incident field $\widehat{E}_{inc}$, the electric field before interacting with any object, and the scattered field $\widehat{E}_{sca}$, the electric field generated due to the interaction with an object, have the relationship $\widehat{E}(r)=\widehat{E}_{inc}+\widehat{E}_{sca}$.

Moreover, $\hat{J}(r)$ is the current, ω is the frequency in radians/second, and i is the classic imaginary unit. Additionally, the domain is $\Omega \subset \mathbb{R}^3$, defined as a convex bounded domain with boundary $\partial\Omega \in C^2$, i.e. the set of continuous functions that have continuous second derivative. It's important to note that (2.6) describes electromagnetic waves propagating through a non-magnetic, homogeneous, and isotropic medium.

Moreover, $\varepsilon_r(r) = \varepsilon(r)/\varepsilon_0$ and $\sigma(r)$ are the relative dielectric permittivity and electric conductivity functions, respectively. The constants ε_0, μ_0 are dielectric permittivity and permeability of free space, respectively, and $c = 1/\sqrt{\varepsilon_0\mu_0}$ is the speed of light in free space.

To further proceed, we'll introduce *the spatially distributed complex dielectric function* $\varepsilon'(r)$,

$$\varepsilon'(r) = \varepsilon_r(r)\frac{1}{c^2} + i\mu_0\frac{\sigma(r)}{\omega} \tag{2.7}$$

this simplification transforms (2.6) to:

$$\nabla \times \nabla \times \widehat{E}(r) - \omega^2\varepsilon'(r)\widehat{E}(r) = i\omega\mu_0\widehat{J}(r). \tag{2.8}$$

Subtracting the term $\nabla \times \nabla \times \widehat{E}(r) - \omega^2\varepsilon_b\widehat{E}(r)$ from both sides of (2.8), and rearranging yields

$$\nabla \times \nabla \times \widehat{E}(r) - \omega^2\left(\varepsilon'(r) - \varepsilon_b\right)\widehat{E}(r) = i\omega\mu_0\widehat{J}(r) + \omega^2\varepsilon_b\widehat{E} \tag{2.9}$$

$$\iff \nabla \times \nabla \times \widehat{E}(r) - \omega^2\varepsilon_b\widehat{E}(r) = i\omega\mu_0\widehat{J}(r) + \omega^2\left(\varepsilon'(r) - \varepsilon_b\right)\widehat{E}(r) \tag{2.10}$$

where ε_b represents the dielectric permittivity corresponding to the background medium.

Before proceeding further, it's necessary to introduce and understand Green's function of a wave equation. Green's function $g(r, r')$ represents the solution of the wave equation for a point source. In the context of an isotropic medium, equation (2.11) is referred to as the inhomogeneous Helmholtz equation [20] [38].

$$\left(\nabla^2 + k^2\right)\widehat{E}\left(r\right) = s\left(r\right). \tag{2.11}$$

Following the convention[1] of [20], we rewrite (2.11) into the form

$$\left(\nabla^2 + k^2\right)g\left(r, r'\right) = -\delta\left(r - r'\right). \tag{2.12}$$

Now from the principle of linear superposition, and since $g(r, r')$ is the solution to (2.11), equation (2.11) has the solution

$$\widehat{E}(r) = -\int \underbrace{g(r, r')}_{=g(r',r)} s(r')dr = -\int g(r - r')s(r')dr = -\int \frac{e^{ik|r-r'|}}{4\pi\left|r - r'\right|}s(r')dr, \tag{2.13}$$

[1] It is highly advisable to read through [13], to understand the details.

k is the k vector denoting the direction of propagation.

This idea can be extended to solve our original problem, that is (2.6). By introducing the dyadic Green's function

$$\bar{G}(r', r) = \bar{G}(r, r') = \left(I + \frac{\nabla' \nabla'}{k^2} \right) g(r, r'), \tag{2.14}$$

where I is the identity operator.

Following [5], we introduce the dyadic Green's function $\bar{G}(r, r')$ for the problem, and follow the convention, i.e

$$\nabla \times \nabla \times \bar{G}(r, r') - \omega^2 \varepsilon_b \bar{G}(r, r') = I\delta(r - r'), \quad r \in \mathbb{R}^3 \tag{2.15}$$

By multiplying (2.10) by $\bar{G}(r, r')$ and (2.15) by $\widehat{E}(r)$, we get:

$$\begin{aligned} \nabla \times \nabla \times \widehat{E}(r)\bar{G}(r, r') - \omega^2 \varepsilon_b \widehat{E}(r)\bar{G}(r, r') = \\ = i\omega\mu_0 \widehat{J}(r)\bar{G}(r, r') + \omega^2 (\varepsilon'(r) - \varepsilon_b) \widehat{E}(r)\bar{G}(r, r') \end{aligned} \tag{2.16}$$

and

$$\nabla \times \nabla \times \bar{G}(r, r')\widehat{E}(r) - \omega^2 \varepsilon_b \bar{G}(r, r')\widehat{E}(r) = \delta(r - r')\widehat{E}(r). \tag{2.17}$$

Then subtracting (2.17) from (2.16) and integrating, we obtain

$$\begin{aligned} \left(\nabla \times \nabla \times \widehat{E}(r), \bar{G}(r, r')\right) - \left(\omega^2 \varepsilon_b \widehat{E}(r), \bar{G}(r, r')\right) - \left(\nabla \times \nabla \times \bar{G}(r, r'), \widehat{E}(r)\right) + \\ + \left(\omega^2 \varepsilon_b \bar{G}(r, r'), \widehat{E}(r)\right) = \\ = \left(i\omega\mu_0 \widehat{J}(r), \bar{G}(r, r')\right) + \left(\omega^2 (\varepsilon'(r) - \varepsilon_b) \widehat{E}, \bar{G}(r, r')\right) - \left(\delta(r - r'), \widehat{E}(r)\right) \\ \iff \left(\nabla \times \nabla \times \widehat{E}(r), \bar{G}(r, r')\right) - \left(\nabla \times \nabla \times \bar{G}(r, r'), \widehat{E}(r)\right) \\ = \left(i\omega\mu_0 \widehat{J}(r), \bar{G}(r, r')\right) + \left(\omega^2 (\varepsilon'(r) - \varepsilon_b) \widehat{E}, \bar{G}(r, r')\right) - \left(\delta(r - r'), \widehat{E}(r)\right), \end{aligned} \tag{2.18}$$

where $(\cdot, \cdot)$ denotes the standard scalar product in space. To further simplify integration by parts is used on the left hand side of (2.18), (see [29]), that is:

$$\left(\nabla \times \nabla \times \widehat{E}(r), \bar{G}(r, r')\right) = \left(\nabla \times \widehat{E}(r), \nabla \times \bar{G}(r, r')\right) \tag{2.19}$$

$$\left(\nabla \times \nabla \times \bar{G}(r, r'), \widehat{E}(r)\right) = \left(\nabla \times \bar{G}(r, r'), \nabla \times \widehat{E}(r)\right). \tag{2.20}$$

Which implies that the left hand side of equation (2.18) is zero, hence now we have

$$\left(i\omega\mu_0 \widehat{J}(r), \bar{G}(r, r')\right) + \left(\omega^2 (\varepsilon'(r) - \varepsilon_b) \widehat{E}, \bar{G}(r, r')\right) - \left(\delta(r - r'), \widehat{E}(r)\right) = 0. \tag{2.21}$$

Rewriting in integral form, and then rearranging and using the principle of linear superposition yields:

$$\widehat{E}(r) = i\omega\mu_0 \int_\Omega \widehat{J}(r)\bar{G}\left(r, r'\right) dr + \omega^2 \int_\Omega \left(\varepsilon'(r) - \varepsilon_b\right) \widehat{E}(r)\bar{G}\left(r, r'\right) dr. \tag{2.22}$$

The first term in the right hand side of (2.22) is the incident electric field $\widehat{E}_{inc}$. Let the object function be $O(r) = \varepsilon'(r) - \varepsilon_b(r)$ so (2.22) further simplifies to

$$\widehat{E}(r) = \widehat{E}_{\text{inc}} + \omega^2 \int_\Omega \widehat{E}(r)O(r) \underbrace{\bar{G}\left(r', r\right)}_{=G(r',r)} dr = \widehat{E}_{\text{inc}} + \widehat{E}_{\text{sca}}, \tag{2.23}$$

where $\widehat{E}_{\text{sca}}$ is the volume integral equation (VIE).

2.2.2 The volume integral equation

The volume integral equation obtained in (2.23) is the mathematical model that we will be working with. Such a volume integral equation is of great use in microwave applications, especially in microwave medical imaging. Due to the Born approximation, i.e. $\widehat{E}(r) \approx \widehat{E}_{inc}(r)$ [5], we can rewrite $\widehat{E}_{sca}(r)$ to

$$\widehat{E}_{sca}(r) = \omega^2 \int_\Omega \bar{G}\left(r', r\right) O(r)\widehat{E}_{inc}(r)dr. \tag{2.24}$$

Moreover, according to [5], (2.24) can be transformed to the following volume integral equation for a bi-static pair of antennas (i, j):

$$S^{sca}_{j,i} = -\frac{\omega^2\varepsilon_b}{4i\omega\mu} \int_\Omega \widehat{E}_{inc,j}(r)O(r)\widehat{E}_{inc,i}(r)dr. \tag{2.25}$$

Notice that $\widehat{E}_{inc,i}(r)$ is the incident electric field produced by the transmitter i, and $\widehat{E}_{inc,j}(r)$ is the incident electric field at the receiver j. Furthermore, $\widehat{E}_{sca}(r)$ is now replaced by the corresponding scattered S-parameter $S^{sca}_{j,i}$, after scaling with the factor $C = -\frac{\omega^2\varepsilon_b}{4i\omega\mu}$. This approach is more suitable for our setup because equation (2.25) uses the scattered S-parameter measurements obtained by a bi-static pair of antennas instead of using the scattered electric field.

As previously mentioned the dielectric problem features an off-centered cylindrical inclusion as the target, serving as the baseline, i.e $t = 0$ for comparing the dynamic cooling process of the heated target at each time step. To simulate the cooling process over a ten-minute period, the dielectric parameters of the target were adjusted through a parametric sweep using CST, as detailed in Table 2.1. Here $\boldsymbol{\epsilon_r(t)}$ is the permittivity at time t and $\boldsymbol{\sigma(t)}$ is the conductivity at time t.

Now, a bounded and linear operator A is introduced to write (2.25) in operator form, that is:

$$A(O) = d, \tag{2.26}$$

where $A(O) = \int_\Omega \widehat{E}_{inc,j}(r)O(r)\widehat{E}_{inc,i}(r)dr$ and $d = S^{sca}_{j,i}$. Notice that equation (2.26) represents a Fredholm integral equation of the first kind [19], and hence can be solved using Tikhonov's functional:

$$J_\alpha(O) = \frac{1}{2}\left\|A(O) - d\right\|_2^2 + \frac{\alpha}{2}\left\|O\right\|_2^2, \tag{2.27}$$

Timeline (min)	$\boldsymbol{\epsilon_r(t)}$	$\boldsymbol{\sigma(t)(\mathbf{S/m})}$
$t = 0$ (baseline)	26	0.12
$t = 2$	28	0.15
$t = 4$	29	0.19
$t = 6$	29.8	0.21
$t = 8$	30.5	0.23
$t = 10$	31	0.24
Coupling fluid 20:7 isopropyl : water ($\epsilon_r = 24.5, \sigma = 0.46$)		

Table 2.1: Changes in permittivity and conductivity of the target as it cools down from 55°C to 29°C over a ten-minute period. This table is directly taken from [3].

since everything is known, that is $\widehat{E}_{inc,j}(r)$, $\widehat{E}_{inc,i}(r)$ and $S^{sca}_{j,i}$, and α is a regularization parameter. We only need to solve for $A(O)$. This can easily be done by minimizing the Tikhonov's functional using basic linear algebra and matrix differentiation. Let us consider the general form $f(x) = \frac{1}{2}\|Ax - b\|_2^2 + \frac{\alpha}{2}\|x\|_2^2$:

$$\begin{aligned} f(x) &= \frac{1}{2}\left((Ax-b)^T(Ax-b) + \alpha x^T x\right) \\ &= \frac{1}{2}\left(x^T A^T Ax - x^T A^T b - b^T Ax + b^T b + \alpha x^T x\right) \\ &= \frac{1}{2}\left(x^T A^T Ax - x^T A^T b - x^T A^T b + b^T b + x^T \alpha I x\right) \\ &= \frac{1}{2}\left(b^T b + -2x^T A^T b + x^T (A^T A + \alpha I)x\right) \end{aligned} \tag{2.28}$$

to minimize $f(x)$ we differentiate and set to zero.

$$\nabla f(x) = \frac{1}{2}\left(-2A^T b + 2(A^T A + \alpha I)x\right) \overset{\text{set}}{=} 0 \tag{2.29}$$

Where we used the classic result from matrix calculus $\frac{\partial x^T Bx}{\partial x} = 2Bx$, where B is a symmetric matrix, solving for $\hat{x} = (A^T A + \alpha I)^{-1} A^T b$. This equation is the solution to the regularized system of normal equations, although they are fast, they can be inaccurate and computationally expensive. To solve these problems, SVD can be used instead [6], that is, let $A = U\Sigma V^T$:

$$\begin{aligned} \hat{x} = \left(A^T A + \alpha I\right)^{-1} A^T b = \\ \left(\left(U\Sigma V^T\right)^T U\Sigma V^T + \alpha I\right)^{-1} \left(U\Sigma V^T\right)^T b = \\ \left(V\Sigma U^T U\Sigma V^T + \alpha I\right)^{-1} V\Sigma U^T b = \\ \left(V\Sigma^2 V^T + \alpha I\right)^{-1} V\Sigma U^T b = \\ = V\left(\Sigma^2 + \alpha I\right)^{-1} \Sigma U^T b. \end{aligned} \tag{2.30}$$

Equation (2.30) is used to reconstruct (2.27), that is $\hat{x} = O$. Another approach is to consider the following Tikhonov's functional

$$M_\alpha(O) = \frac{1}{2} \|A(O) - d\|_2^2 + \frac{\alpha}{2} \|O\|_{H^1}^2 , \tag{2.31}$$

That is, using the H^1-norm instead of the L_2-norm. To solve the regularized least-squares problem in the H^1 norm, we start with the generalized objective function:

$$f(x) = \frac{1}{2}\|Ax - b\|_2^2 + \frac{\alpha}{2}\|x\|_{H^1}^2. \tag{2.32}$$

Using the definition of the H^1 norm [17]:

$$\|x\|_{H^1}^2 = \|x\|_2^2 + \|\nabla x\|_2^2, \tag{2.33}$$

we can rewrite the objective function as:

$$f(x) = \frac{1}{2}\|Ax - b\|_2^2 + \frac{\alpha}{2}\left(\|x\|_2^2 + \|\nabla x\|_2^2\right). \tag{2.34}$$

To find the minimum of $f(x)$, we take the derivative with respect to x and set it to zero:

$$\nabla f(x) = A^T(Ax - b) + \alpha x - \alpha \Delta x = 0, \tag{2.35}$$

where we used the identity [1]:

$$\frac{\partial}{\partial x}\left(\frac{\alpha}{2}\|\nabla x\|_2^2\right) = -\alpha \Delta x. \tag{2.36}$$

This leads to the equation:

$$A^T Ax - A^T b + \alpha x - \alpha \Delta x = 0. \tag{2.37}$$

Rearranging, we get:

$$(A^T A + I - \alpha \Delta)x = A^T b. \tag{2.38}$$

Solving for x, we have:

$$\hat{x} = (A^T A + I - \alpha \Delta)^{-1} A^T b. \tag{2.39}$$

In the context of the SVD decomposition, we express A using its SVD: $A = U\Sigma V^T$. Substituting this into the equation, we get:

$$\hat{x} = V\left(\Sigma^2 + \alpha\left(I - \Delta\right)\right)^{-1} \Sigma U^T b. \tag{2.40}$$

To obtain an even more robust solution, we can introduce another regularization parameter, resulting in:

$$\hat{x} = V\left(\Sigma^2 + (\alpha_1 I - \alpha_2 \Delta)\right)^{-1} \Sigma U^T b. \tag{2.41}$$

where Δ is the Laplace operator. It is worth mentioning that while calculating the Laplace operator is discretized, see for example [6] for details. For another approach see [3], where Fréchet derivatives are utilized.

2.2.3 Tikhonov's regularizations methods

Now that we have 3 different ways of reconstructing: (2.30), (2.40) and (2.41), all that is left is to optimize the regularization parameters. To do so, we'll use three different approaches: *L-curves*, *Morozov's discrepancy principle* and *the balancing principle: fixed point algorithm*.

Starting with L-curves, they are a convenient way of displaying the trade-off between the logarithmic norm of the solution $\|x\|_2$ and the logarithmic norm of the residual $\|Ax - b\|_2$, representing the compromise between minimizing these two quantities. Moreover, L-curves indicate whether the norms are unreasonably large or small. Therefore, they serve as an initial guideline for identifying an optimal regularization parameter. Here, we will not delve too deeply into the theory, see [21, 10, 37, 22].

Next is Morozov's discrepancy principle. The core idea behind it is rather simple: one loops through a range of equidistant regularization parameters, and the ones that give the smallest residual are considered the best regularization parameters, see Algorithm 1.

Algorithm 1: Morozov's discrepancy principle

Input : V, Σ, U, b: Matrices and vector
Input : α_{initial}: Initial value of regularization parameter
Input : α_{last}: Last value of regularization parameter
Output: M: Updated reconstruction matrix
Output: α: Final regularization parameter

for α *in* $[\alpha_{initial}, \alpha_{last}]$ **do**
    Calculate $M =$ from (2.30) or (2.40) or (2.41);
    Calculate $[V, \Sigma, U] = \text{svd}(M)$;
    Calculate the Moore–Penrose inverse of M: $M^+ = \text{pinv}(M)$;
    Calculate the residual: $\text{Res} = \|M^+ b - b\|_2$;
end
The best regularization parameter α is the one with the smallest residual;

As seen in Algorithm 1, the vector b and the SVD of the reconstruction of matrix M are known, while the rest of the parameters are chosen. The reason for using singular value decomposition here is its computational efficiency; it is less expensive computationally. Furthermore, we use the Moore-Penrose inverse because the rank of M is not full. Repeat the algorithm while keeping track of each residual. The α that corresponds to the smallest residual is the best α, as it yields the smallest error. It is worth noting that when the reconstruction (2.41) is employed, one loops through a range of values for two α parameters.

Our next algorithm is the *balancing principle: fixed point algorithm.*

Algorithm 2: Balancing principle: fixed point algorithm

Input : V, Σ, U, b: Matrices and vector
Input : n: Number of iterations
Input : α_{initial}: Initial value of regularization parameter
Output: M: Updated reconstruction matrix
Output: α: Final regularization parameter

```
Initialize M with the initial guess;
Initialize α with α_initial;
for k = 1 to n do
    Calculate M = from (2.30) or (2.40) or (2.41);
    Compute SVD: [V, Σ, U] = svd(M);
    Calculate φ_k = VΣ²V^T Mb − VΣU^T b;
    Update α_k = ||φ_k||_2 / ||Mb||_2;
    Update M with the new α_k ;
    if convergence then
        break;
    end
end
```

It is worth noting that when the reconstruction (2.41) is employed, we initially use the reconstruction (2.40) set the optimal regularization parameter as α_1 or α_2 and then repeat the algorithm again. To prove the convergence of the fixed point algorithm, as seen in [24], we introduce and demonstrate the balancing principle rule. Thereafter, we prove the fixed point algorithm. First, let's introduce some new notation. We denote the general Tikhonov functional as follows:

$$J_\alpha(x) = \frac{1}{2}\|F(x) - y\|_2^2 + \alpha\psi(x) \tag{2.42}$$

$$= \phi(x) + \alpha\psi(x). \tag{2.43}$$

Also define $\bar{\psi}(\alpha)$ and $\bar{\phi}(\alpha)$ as

$$\bar{\psi}(\alpha) = F'(\alpha), \tag{2.44}$$

$$\bar{\phi}(\alpha) = F(\alpha) - \alpha F'(\alpha). \tag{2.45}$$

Moreover, let D^+ and D^- be definition of the one-sided derivatives:

$$D^- F(\alpha) = \lim_{h \to 0^+} \frac{F(\alpha) - F(\alpha - h)}{h}, \tag{2.46}$$

$$D^+ F(\alpha) = \lim_{h \to 0^+} \frac{F(\alpha + h) - F(\alpha)}{h}. \tag{2.47}$$

The balancing principle rule:

$$\bar{\phi}(\alpha) = \gamma \alpha \bar{\psi}(\alpha), \tag{2.48}$$

finds $\alpha > 0$ such that the following function is minimized:

$$\Phi_\gamma(\alpha) = \frac{F^{1+\gamma}(\alpha)}{\alpha}. \tag{2.49}$$

where $\gamma = \frac{a_0}{a_1}$ is determined by the statistical a priori knowledge from shape parameters in Gamma distributions. When $\gamma = 1$ the method is called the *zero-crossing method*, see for example [25].

Using the definitions (2.44) and (2.45), the balancing equation (2.48) becomes:

$$\begin{aligned} 0 &= \bar{\phi}(\alpha) - \gamma \alpha \bar{\psi}(\alpha) \\ &= F(\alpha) - \alpha F'(\alpha) - \gamma \alpha F'(\alpha) \\ &= F(\alpha) - \alpha F'(\alpha)(1 + \gamma) \\ &\iff F(\alpha) = \alpha F'(\alpha)(1 + \gamma) \end{aligned} \tag{2.50}$$

Moreover, (2.50) is equivalent to

$$\frac{1}{\alpha} = \frac{F'(\alpha)}{F(\alpha)}(1 + \gamma) = \frac{\frac{dF}{d\alpha}}{F(\alpha)}(1 + \gamma) \quad \text{or} \quad \frac{d\alpha}{\alpha} = \frac{dF}{F(\alpha)}(1 + \gamma). \tag{2.51}$$

Integrating both sides of (2.51), and letting $C_1 = C_2$

$$\begin{aligned} \ln \alpha + C_1 &= (1 + \gamma) \ln F(\alpha) + C_2 \\ \alpha &= \exp\left((1 + \gamma) \ln F(\alpha)\right) = F(\alpha)^{1+\gamma}, \end{aligned} \tag{2.52}$$

dividing by α we can rewrite (2.52) as the function to be minimized in the balancing principle

$$\Phi_\gamma(\alpha) = \frac{F^{1+\gamma}(\alpha)}{\alpha} = 1. \tag{2.53}$$

Taking the derivative one can check that the minimum of $\Phi_\gamma(\alpha)$ is at

$$0 = \left(\Phi_\gamma(\alpha)\right)' = \frac{(1 + \gamma) F'(\alpha) F^\gamma(\alpha) \alpha - F^{1+\gamma}(\alpha)}{\alpha^2} \tag{2.54}$$

simplifying further one obtains:

$$(1 + \gamma) F'(\alpha) F^\gamma(\alpha) \alpha = F^{1+\gamma}(\alpha) \implies (1 + \gamma) F'(\alpha) \alpha = F(\alpha). \tag{2.55}$$

Which is the same equation as (2.50) and hence also $\bar{\phi}(\alpha) = \gamma \alpha \bar{\psi}(\alpha)$ Therefore, the balancing principle calculates the optimal value of α when $\left(\Phi_\gamma(\alpha)\right)' = 0$.

Now we are ready to prove the local convergence of the fixed point algorithm, (Algorithm 2). However, before proceeding, we need to introduce an assumption and a lemma. Let's begin with the assumption:

Assumption 2.2.1. *Let the interval* $[\zeta_0, \zeta_1]$ *satisfy:*

(a) $\bar{\psi}(\zeta_1) > 0$*;*

(b) There exists an optimal parameter α_b *in* $[\zeta_0, \zeta_1]$ *such that* $D^{\pm}\Phi_\gamma(\alpha) < 0$ *for* $\zeta_0 \leq \alpha < \alpha_b$ *and* $D^{\pm}\Phi_\gamma(\alpha) > 0$ *for* $\alpha_b < \alpha \leq \zeta_1$.

Using Assumption 2.2.1, one can guarantee the well-posedness of the algorithm. We can now state the following lemma, which is essential for proving the fixed-point algorithm.

Lemma 2.2.1. *Let Assumption 2.2.1 hold, and* $\alpha_0 \in [\zeta_0, \zeta_1]$*. Then the sequence* $\{\alpha_k\}_k$ *generated by Algorithm 2 satisfies:*

1. *It is either finite or infinite and strictly monotone, and increasing (decreasing) if* $r(\alpha_0) > 0$ $(r(\alpha_0) < 0)$*,*
2. *It is contained in* $[\zeta_0, \alpha_b]$ $([\alpha_b, \zeta_1])$ *if* $r(\alpha_0) > 0$ $(r(\alpha_0) < 0)$.

for a proof of Lemma 2.2.1 see [24].

Now we have everything we need to show the convergence of the fixed point algorithm:

Theorem 2.2.2. *Let Assumption 2.2.1 hold, and* $\alpha_0 \in [\zeta_0, \zeta_1]$*. Then the following statements hold for the sequence* $\{\alpha_k\}$ *generated by Algorithm 2*

a The sequence $\{\Phi_\gamma(\alpha_k)\}$ *is monotonically decreasing.*

b The sequence $\{\alpha_k\}$ *converges to the local minimizer* α_{b}.

Proof. Let us define the residual $r(\alpha) = \bar{\phi}(\alpha) - \gamma\alpha\bar{\psi}(\alpha)$. We focus on the case $r(\alpha_0) > 0$. Then the sequence $\{\alpha_k\}$ is increasing, consider the case $\alpha_k < \alpha_{k+1}$. The function F is concave and thus Lipschitz continuous (see for example [16]), and thus $\Phi_\gamma(\alpha)$ is locally Lipschitz continuous. Moreover, $\Phi'_\gamma = \frac{F(\alpha)^\gamma}{\alpha^2}(-r(\alpha))$ exists almost everywhere since

$$\begin{aligned}\frac{(1+\gamma)F^\gamma(\alpha)F'(\alpha)\alpha - F^{1+\gamma}(\alpha)}{\alpha^2} &= \left(\frac{F(\alpha)^\gamma((1+\gamma)F(\alpha)\alpha - F(\alpha))}{\alpha^2}\right) \\ &= \frac{F(\alpha)^\gamma}{\alpha^2}(-r(\alpha)) < 0\end{aligned}$$

and it is locally integrable. Therefore, the following identity holds

$$\Phi_\gamma(\alpha_{k+1}) = \Phi_\gamma(\alpha_k) + \int_{\alpha_k}^{\alpha_{k+1}} \Phi'_\gamma(\alpha)d\alpha, \tag{2.56}$$

and since $\Phi'_\gamma(\alpha) < 0$ then (2.56) implies $\Phi_\gamma(\alpha_{k+1}) < \Phi_\gamma(\alpha_k)$ and thus the sequence $\{\Phi_\gamma(\alpha_k)\}$ is monotonically decreasing, which shows part *a*.

By Lemma 2.2.1, there exists a limit $\alpha^* \in [\zeta_0, \zeta_1]$. If $\alpha_k < \alpha_{k+1}$ then
$\Phi_\gamma(\alpha_{k+1}) < \Phi_\gamma(\alpha_k)$ (since it's monotonically decreasing). For the finite sequence

$\{\alpha_k\}_{k=k_0}^{1}$ it hold that:

$$\lim_{k\to k_0} D^{+}\Phi_\gamma(\alpha_k) \leq \lim_{k\to k_0} \frac{F^\gamma(\alpha_k)}{\alpha_k^2}(-r(\alpha_k)) \leq \lim_{k\to k_0} D^{-}\Phi_\gamma(\alpha_k).$$

then $D^{\pm}\Phi_\gamma(\alpha_{k_0}) = 0$ since $-r(\alpha_{k_0}) = 0$. By Assumption 2.2.1, this local minimizer $\alpha_{k_0} = \alpha_b$. Now from iterations in the fixed point algorithm we have:

$$\begin{aligned} \frac{1}{\gamma}\frac{F\left(\alpha_k\right) - \alpha_k D^{-}F\left(\alpha_k\right)}{D^{-}F\left(\alpha_k\right)} &\leq \alpha_{k+1} = \frac{1}{\gamma}\frac{\bar{\phi}\left(\alpha_k\right)}{\bar{\psi}\left(\alpha_k\right)} \\ &\leq \frac{1}{\gamma}\frac{F\left(\alpha_k\right) - \alpha_k D^{+}F\left(\alpha_k\right)}{D^{+}F\left(\alpha_k\right)}. \end{aligned} \tag{2.57}$$

Since $\lim_{k\to\infty} D^{\pm}F(\alpha_k) = D^{-}F(\alpha^*)$ and the local minimizer $\alpha_b = \alpha^*$, we have

$$\alpha^* = \frac{1}{\gamma}\frac{F(\alpha^*) - \alpha^* D^{-}F(\alpha^*)}{D^{-}F(\alpha^*)},$$

and hence, the limit α^* is the local minimizer α_{b} [24]. This shows part b and hence proves the theorem. ■

Now that we've proved the convergence of the fixed point algorithm, we'll use the SVD to rewrite $\bar{\psi}(\alpha)$ and $\bar{\phi}(\alpha)$. Using a similar approach as in the derivation of (2.30), that is, starting in a similar fashion as in (2.28), one arrives at:

$$\bar{\phi}(\alpha) = V\Sigma^2 V^T Mb - VSU^T b \tag{2.58}$$

$$\bar{\psi}(\alpha) = Mb \tag{2.59}$$

where M is a given reconstruction, that is (2.30), (2.40) or (2.41).

3
Results

The results are presented in two different formats: the first is a three dimensional view, and the second is a two dimensional view, that is $|O| = \sqrt{Re(O)^2 + Im(O)^2}$. Where Re and Im are the real and the imaginary part of O, respectively. Figures 3.1 and 3.2 show these reconstructions using (2.30). Moreover, since Equation (2.41) is a generalization of Equation (2.40), the focus is mostly on Equation (2.41). The reconstructions are seen in Figures 3.3 and 3.4. Two things are observed: firstly, the background of the reconstruction is slightly smoother, but most importantly is the importance of the regularization parameter. As seen in Figures 3.3 and 3.4, with $\alpha_1 = 1$ and $\alpha_2 = 1$, the result are sub-optimal. This can even be observed in the first case, i.e. Figures 3.1 and 3.2. Despite us getting heat, it is not optimized at all.

Moreover, this section is split into three parts: Test 1, where the results of the L-curves are presented. Test 2, where the results of Morozov's discrepancy principle and lastly, Test 3, where the results of the balancing principle are presented.

The code can be found at the link given in [28].

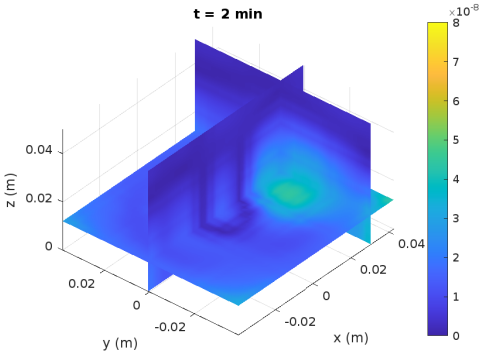

(a) Time step 1

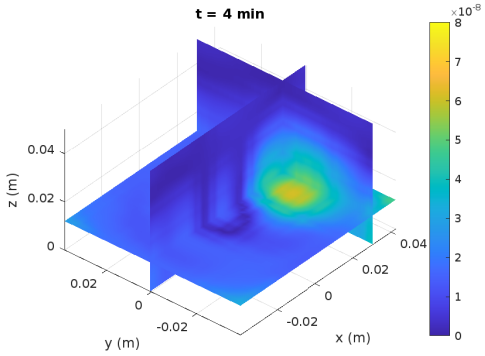

(b) Time step 2

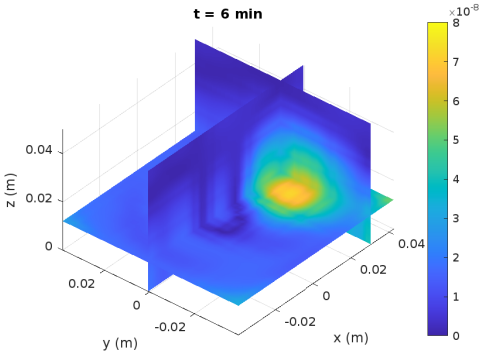

(c) Time step 3

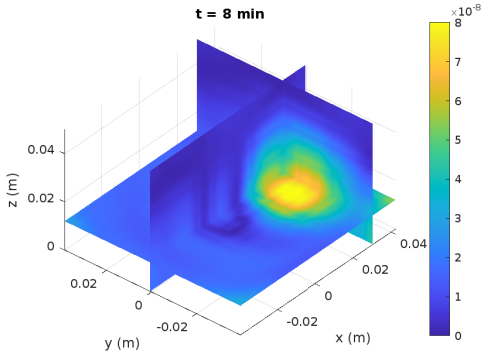

(d) Time step 4

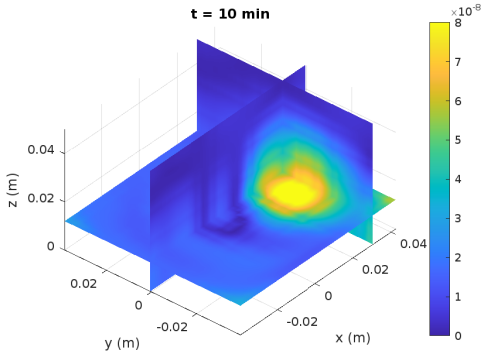

(e) Time step 5

Figure 3.1: Test 1 and Test 3: Reconstruction using (2.30) with the regularization parameter $\alpha = 1$ in three dimensions at each time step.

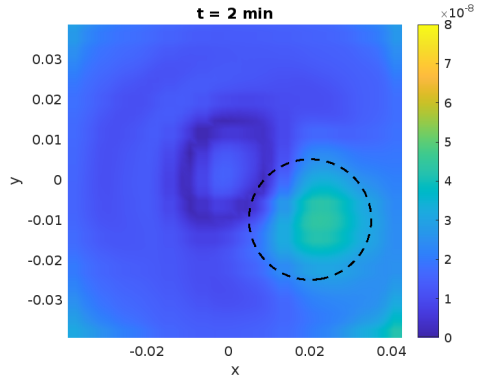

(a) Time step 1

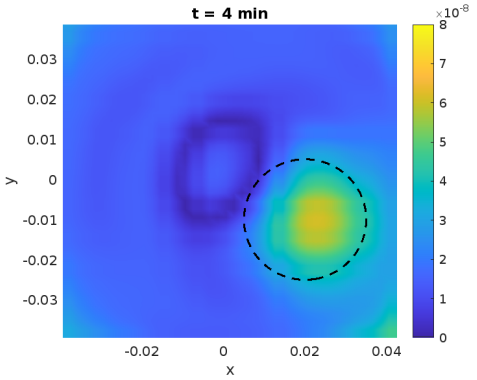

(b) Time step 2

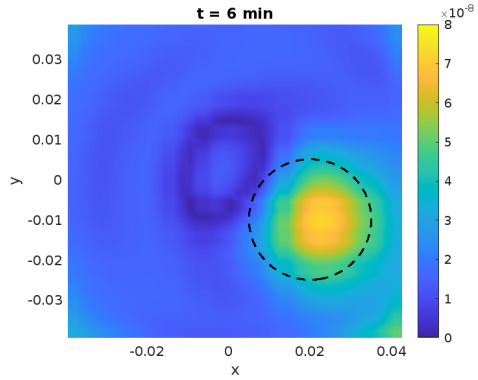

(c) Time step 3

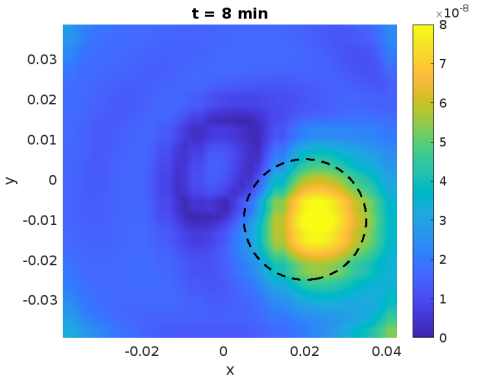

(d) Time step 4

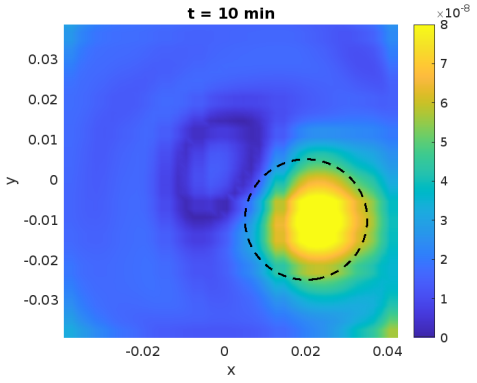

(e) Time step 5

Figure 3.2: Test 1 and Test 3: Two dimensional view of the reconstruction (2.30) with $\alpha = 1$ at each time step.

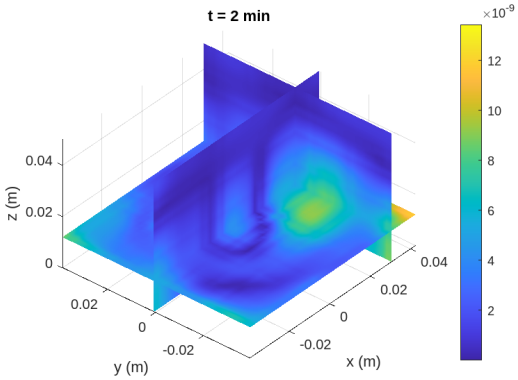

(a) Time step 1

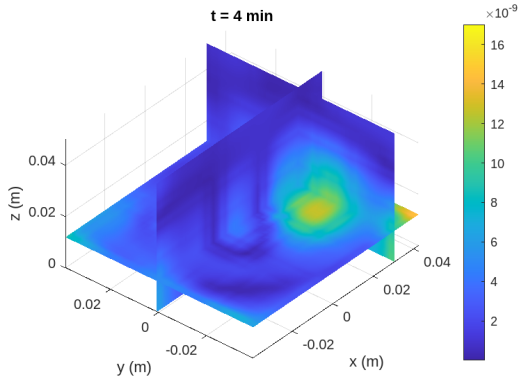

(b) Time step 2

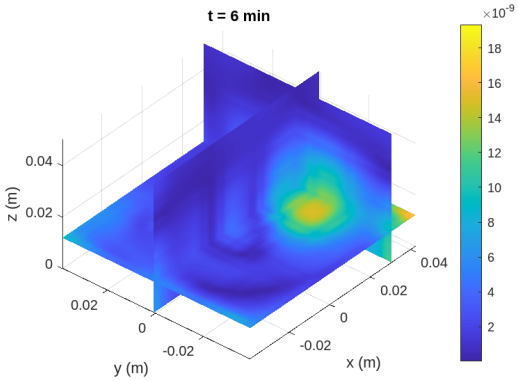

(c) Time step 3

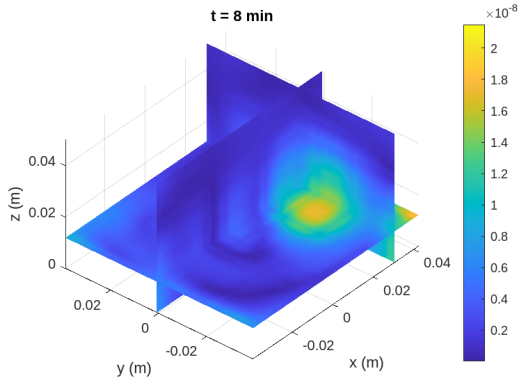

(d) Time step 4

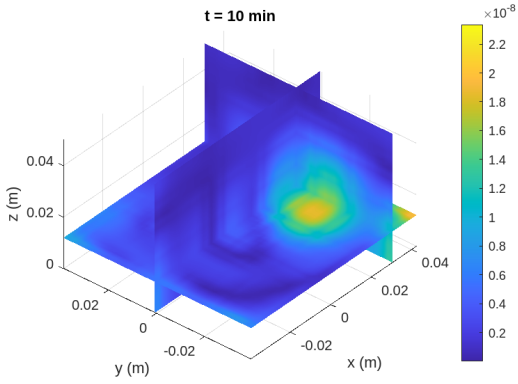

(e) Time step 5

Figure 3.3: Test 1 and Test 3: Reconstruction using (2.41) with $\alpha_1 = 1$ and $\alpha_2 = 1$ in three dimensions at each time step.

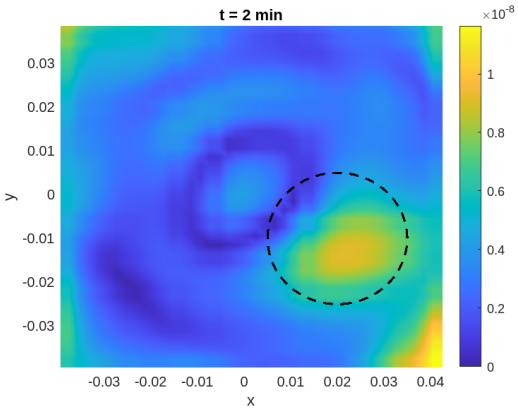

(a) Time step 1

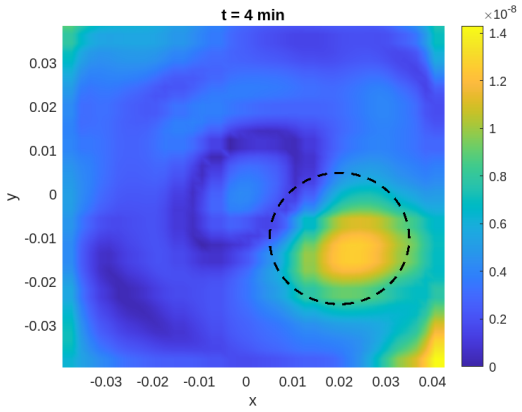

(b) Time step 2

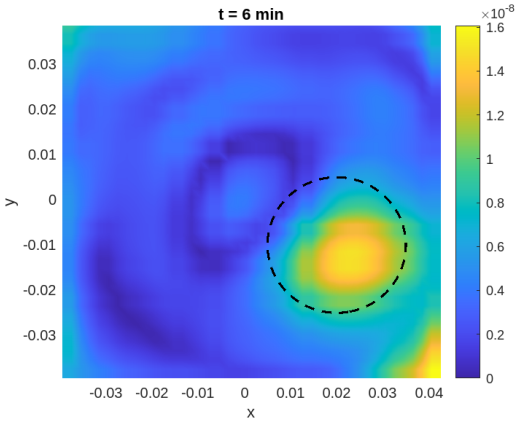

(c) Time step 3

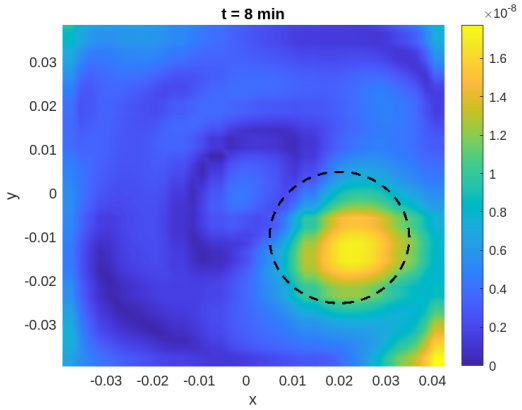

(d) Time step 4

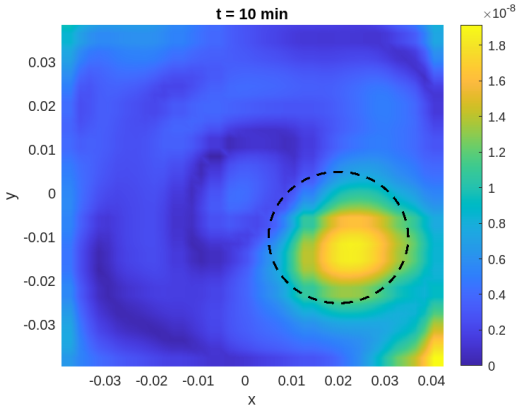

(e) Time step 5

Figure 3.4: Test 1 and Test 3: Two dimensional view of the reconstruction (2.41) with $\alpha_1 = 1$ and $\alpha_2 = 1$ at each time step.

3.1 Test 1: L-curves

Let's begin analyzing the L-curves to gain insight into what potential α-values might be optimal.

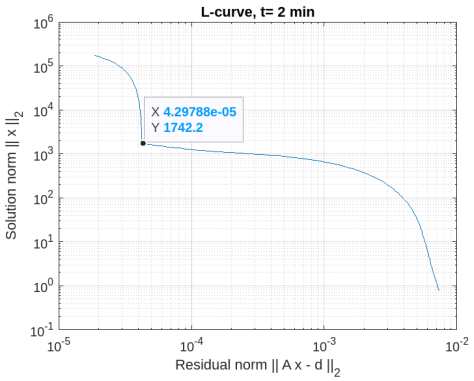

(a) Time step 1

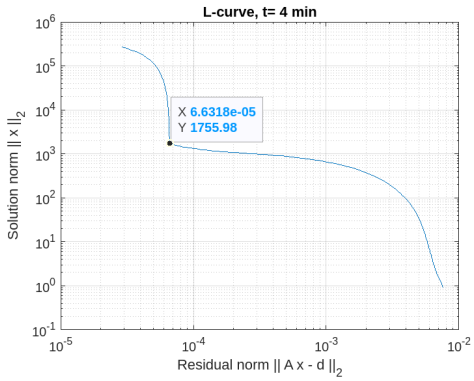

(b) Time step 2

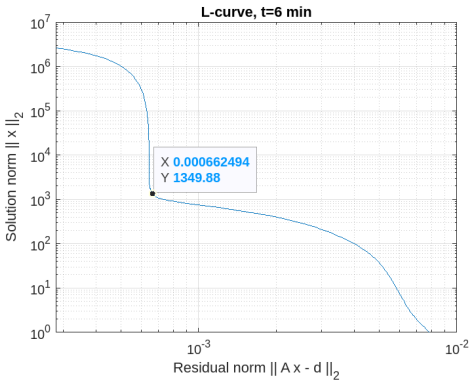

(c) Time step 3

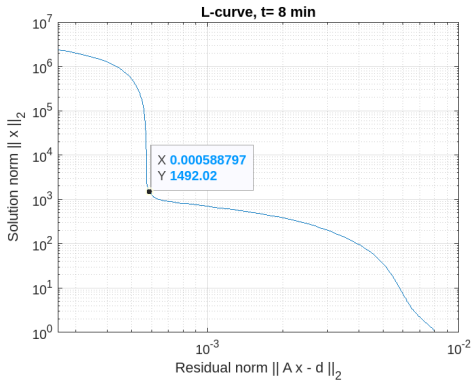

(d) Time step 4

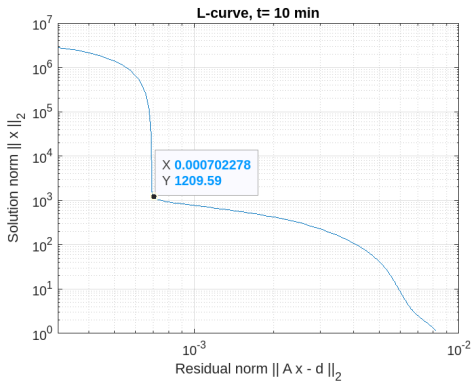

(e) Time step 5

Figure 3.5: L-curve plots for all time steps, using the reconstruction (2.30).

Figure 3.5 displays the L-curves for all time steps. On the x-axis, the logarithmic (second) norm of the residual, while the y-axis is the logarithmic norm of the solution. The optimal value is displayed at the highlighted corner, where the x-value is the optimal regularization parameter value. Converting the optimal values, we see that they are all close to 1. This means that an initial optimal value for the

reconstruction (2.30) is 1, independent of the time step. Unfortunately, the current L-curve cannot be used for the reconstruction (2.41), as it involves two regularization parameters. This implies the need for a three dimensional L-curve, which has not been implemented. However, if the L-curve is implemented on the reconstruction (2.40) the optimal values are also 1. All of these reconstructions are seen in Figure 3.1,3.2, 3.3 and 3.4.

3.2 Test 2: Morozov's discrepancy principle

Starting with the reconstruction (2.30), running Algorithm 1 one obtains the results seen in Table 3.1, where α_0 is the initial guess, α_{last} is the last point on the interval and α^* is the optimal, i.e. with the lowest residual $\|M^+b - b\|_2$. The top-down view and the three dimensional reconstruction are seen in Figure 3.6 and 3.7, respectively.

Time step	α_0	α_{last}	α^*
1	0.3	0.5	0.430
2	0.4	0.7	0.59
3	0.45	0.8	0.7
4	0.45	0.8	0.69
5	0.49	0.9	0.77

Table 3.1: The obtained results for Algorithm 1 and the reconstruction (2.30), where α_0 is the initial guess, α_{last} is the last point on the interval and α^* is the optimal, i.e. with the lowest residual $\|M^+b - b\|_2$.

The same approach can be applied to the reconstruction (2.41). To emphasize, Algorithm 1 is looped through two ranges: one for α_1 and another for α_2. This process yields the results shown in Table 3.2, where α_0 is the initial guess for both α_1 and α_2, α_{last} is the last point on the intervals and (α_1^*,α_2^*) is the optimal pair of values. The top-down view and the three dimensional reconstruction are seen in Figure 3.8 and 3.8, respectively.

Time step	α_0	α_{last}	$(\alpha_1^*$, $\alpha_2^*)$
1	0.09	0.15	(0.150, 0.100)
2	0.1	0.2	(0.150, 0.120)
3	0.1	0.3	(0.130, 0.180)
4	0.14	0.25	(0.230, 0.190)
5	0.14	0.25	(0.230, 0.170)

Table 3.2: Results for Algorithm 1 applied to the reconstruction (2.41), where α_0 is the initial guess for both α_1 and α_2, α_{last} is the last point on the intervals and (α_1^*,α_2^*) is the optimal pair of values, i.e. with the lowest residual $\|M^+b - b\|_2$.

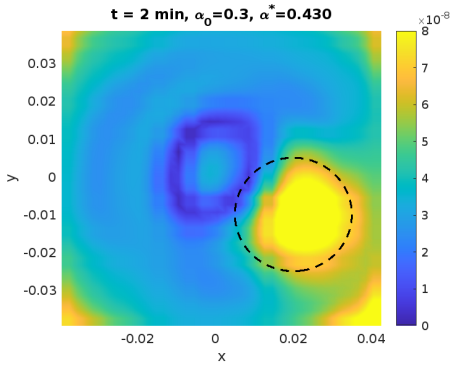

(a) Time step 1

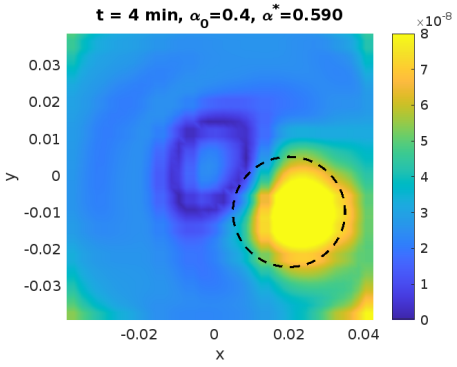

(b) Time step 2

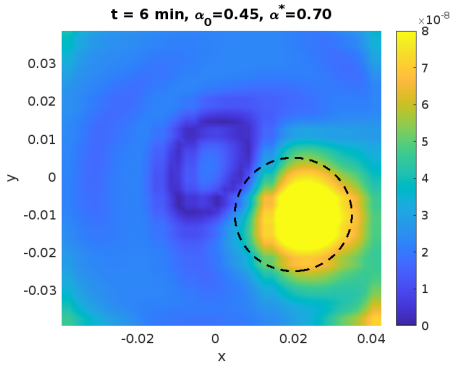

(c) Time step 3

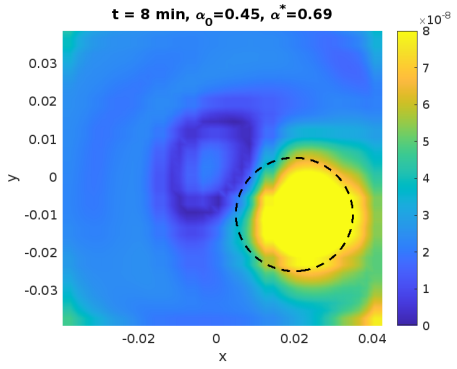

(d) Time step 4

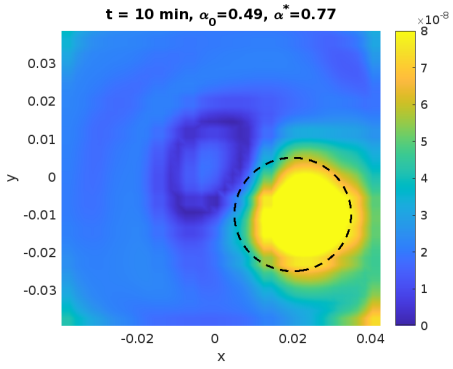

(e) Time step 5

Figure 3.6: Test 2: Morozov's discrepancy principle according to Table 3.1. The two dimensional view of the reconstruction (2.30) is displayed.

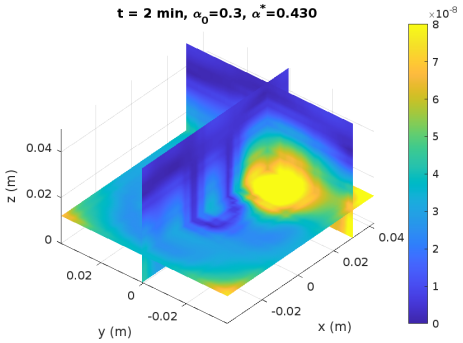

(a) Time step 1

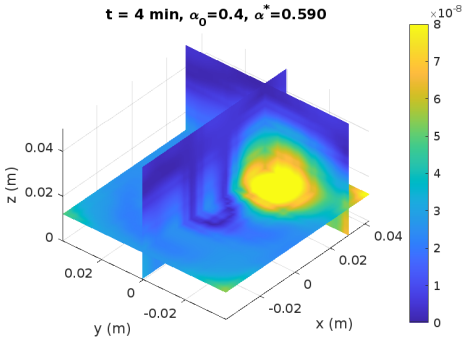

(b) Time step 2

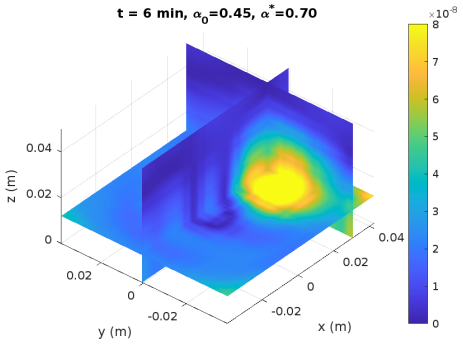

(c) Time step 3

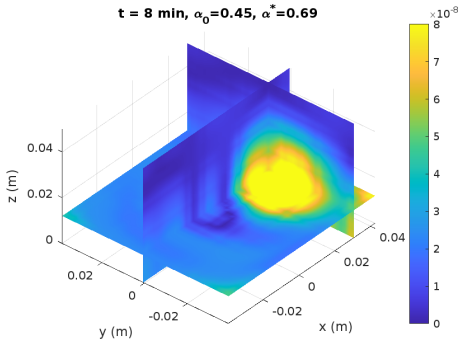

(d) Time step 4

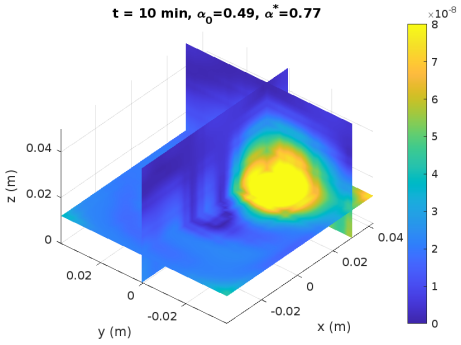

(e) Time step 5

Figure 3.7: Test 2: Morozov's discrepancy principle according to Table 3.1. The three dimensional view using the reconstruction (2.30) is displayed.

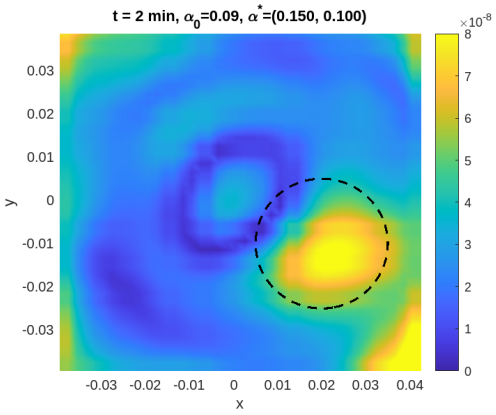

(a) Time step 1

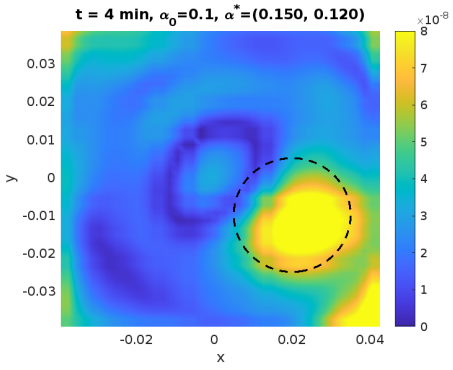

(b) Time step 2

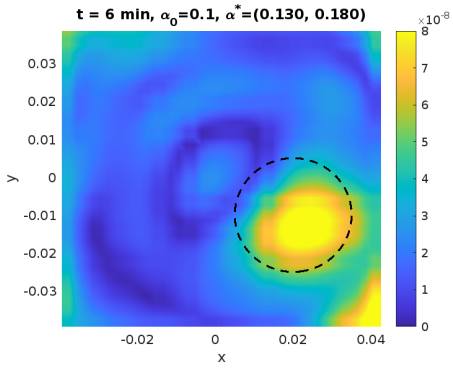

(c) Time step 3

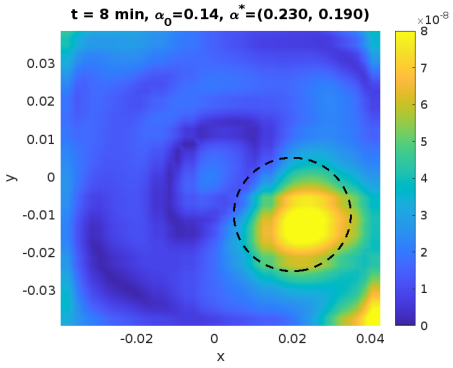

(d) Time step 4

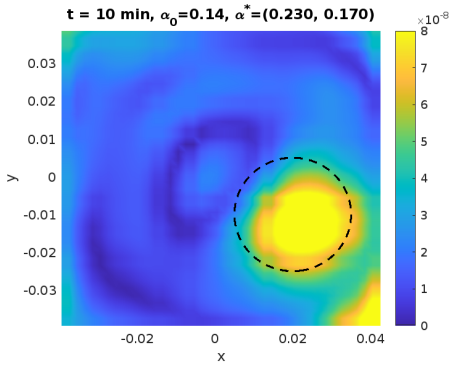

(e) Time step 5

Figure 3.8: Test 2: Morozov's discrepancy principle according to Table 3.2. The two dimensional view of the reconstruction (2.41) is displayed.

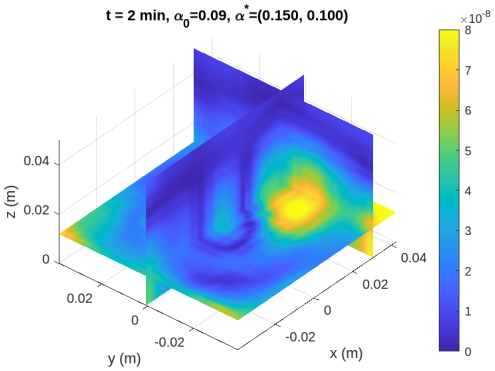

(a) Time step 1

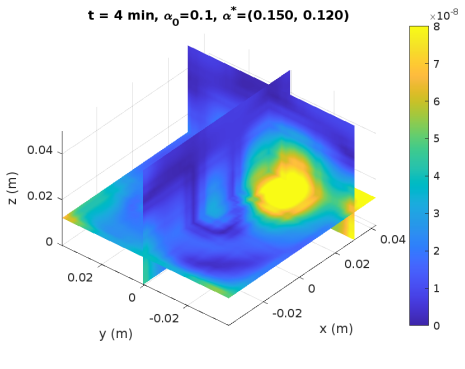

(b) Time step 2

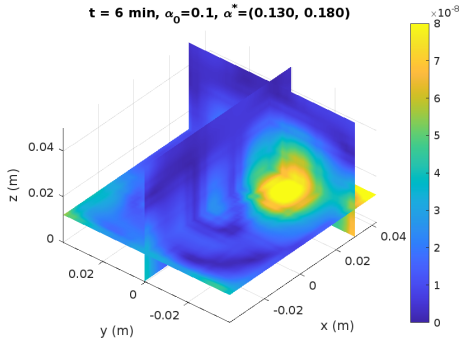

(c) Time step 3

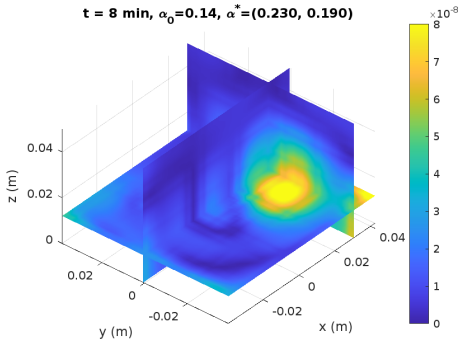

(d) Time step 4

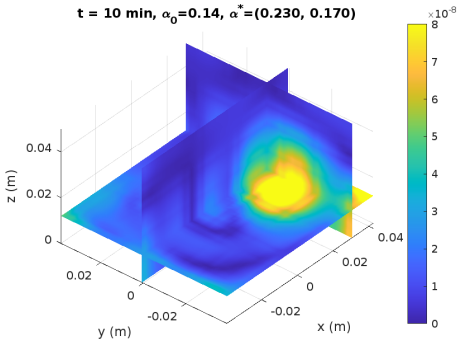

(e) Time step 5

Figure 3.9: Test 2: Morozov's discrepancy principle according to Table 3.2. The three dimensional view using the reconstruction (2.41) is displayed.

The scenario where $\alpha_1 = 0$ in (2.41) was also considered. However, this consistently yielded poor results, as illustrated in Figure 3.10. Even after selectively choosing values to avoid poor outcomes, see Figure 3.11, the results remained unsatisfactory. Consequently, this case was disregarded and not considered further. Nonetheless, this scenario highlighted the importance of initial values and demonstrated how significantly outcomes can be affected.

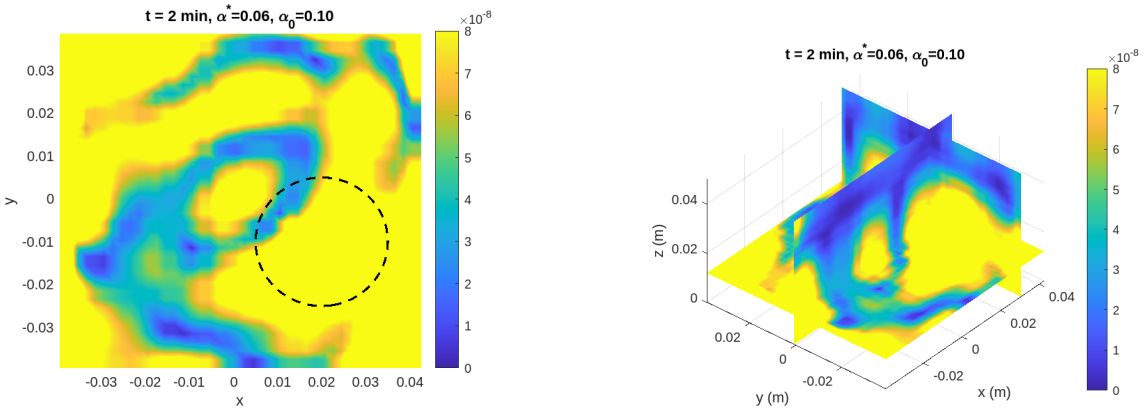

(a) Time step 1 **(b)** Time step 1 (3D)

Figure 3.10: Two and three dimensional view of Morozov's discrepancy principle for the reconstruction (2.41) at Time step 1, with $\alpha_1 = 0$ and optimal value $\alpha_2^* = 0.060$ and a starting value $\alpha_{2_0} = 0.010$.

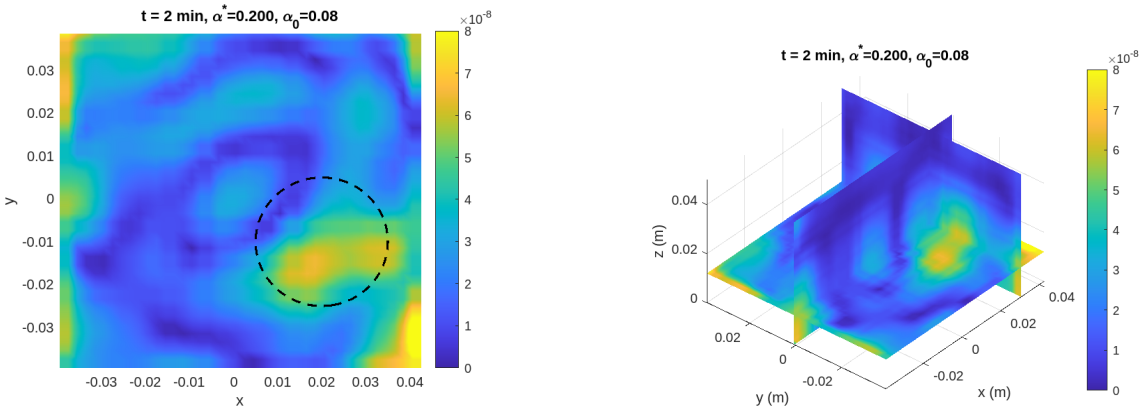

(a) Time step 1 **(b)** Time step 1 (3D)

Figure 3.11: Two and three dimensional view of Morozov's discrepancy principle for the reconstruction (2.41) at Time step 1, with $\alpha_1 = 0$ and optimal value $\alpha_2^* = 0.2$ and a starting value $\alpha_{2_0} = 0.08$.

3.3 Test 3: the balancing principle

The balancing principle: fixed point algorithm (Algorithm 2) was employed on the reconstruction (2.30) and yielded the results shown in Figure 3.12. For the reconstruction (2.41), $\alpha_1 = 1$ was chosen based on the previous observations. Running the fixed point algorithm in this case yielded similar results to those in Figure 3.12, with all values converging to approximately 1. This is an acceptable value, and the reconstructions can be seen in Figures 3.1, 3.2, 3.3, and 3.4.

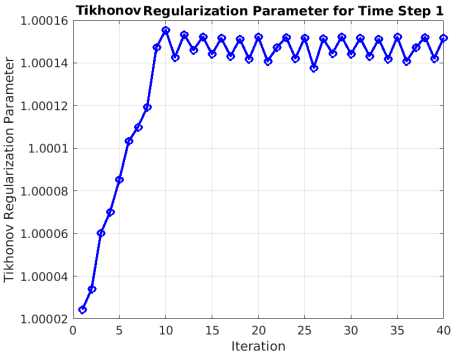

(a) Time step 1

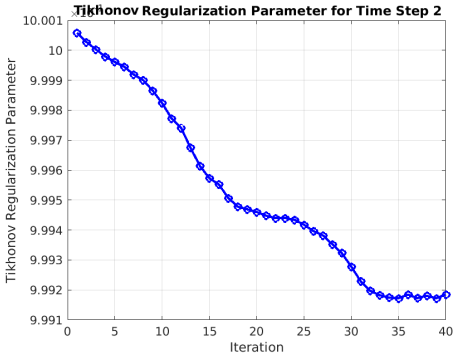

(b) Time step 2

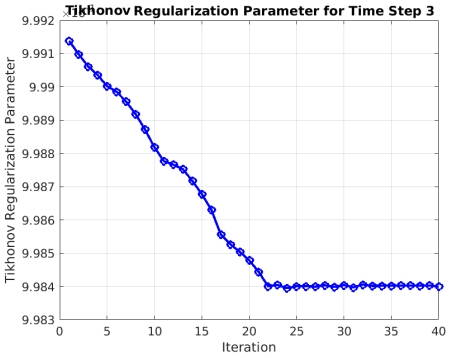

(c) Time step 3

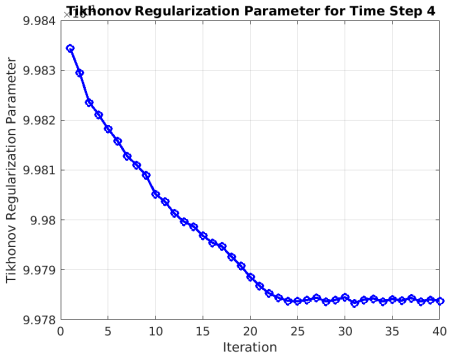

(d) Time step 4

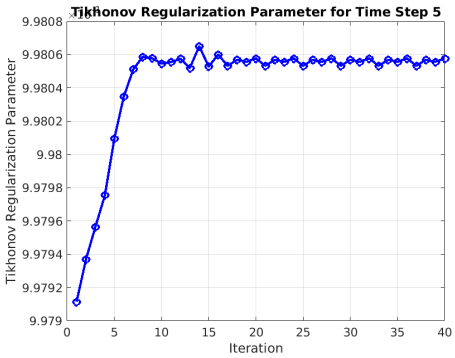

(e) Time step 5

Figure 3.12: The convergence of the Tikhonov regularization parameters for the fixed point algoeithm (Algorithm 2) for all time steps.

4

Discussion and Conclusion

In this study, we aimed to find the best method for optimizing the regularization parameter for Tikhonov's functional, which originated from a partial differential equation and was further transformed into a volume integral equation. This equation was solved using Tikhonov's functionals, which provided us with three different approaches for reconstructing the dielectric problem. Depending on the reconstruction method, the number of regularization parameters varied. To find the optimal regularization parameters, three methods were employed, each showing different results.

The L-curves and the fixed point algorithm yielded similar results, indicating that 1 is the best regularization parameter, which is an acceptable value, as seen in Figures 3.1, 3.2, 3.3, and 3.4, both yeilding an error of order 10^{-1}. However, using Morozov's discrepancy principle, we obtained better results, as seen in Figures 3.6, 3.7, 3.8, 3.9, all yielding an error of order 10^{-2} to 10^{-3}. The major drawback with Morozov's discrepancy principle is the importance of the initial reconstruction matrix. If one does not choose a good reconstruction matrix, the output may look like Figure 3.10 and even after carefully and tediously optimizing by hand by choosing different reconstruction matrices as the initial estimate, one may still obtains a rather poor solution, as seen in Figure 3.11.

Several different attempts were employed to resolve that issue. Among these were the introduction of boundary conditions either to the original PDE (2.6) or when minimizing Tikhonov's functionals. This approach is feasible since the solution on the boundary is known. One attempt was to set the minimal value of the solution on the border. Another was taking the simplest case, the max-norm (i.e the L_1-norm) and then setting the constraints. A completely different approach was to introduce a delta-function such that Morozov's discrepancy principal (Algorithm 1) is only applicable in the region of interest, the smaller inner circle. This approach did yield "optimal" results, meaning the area of interest was completely heated while the background was not. That is, the cancerous cell was completely dead while the healthy tissues around it were not heated at all. However, this approach was completely unrealistic and very hard-coded to obtain a desired result.

In conclusion, the best algorithm to use is Morozov's discrepancy principle. However, in its current form, it is not applicable in real-life scenarios because it requires extensive adjustments to the initial guess. As previously mentioned, setting up a good set of constraints should resolve this issue.

When it comes to the different methods of reconstruction, it is evident that the simple L_2-norm is the best approach. Both of the other methods, the mixed L_2-norm and H^1-norm were less effective. Although the H^1-norm resulted in fewer artifacts in the background, it did not concentrate the heat on the cancerous cell effectively.

One of the aims of this project was to compare the FEM utilized in earlier research [3, 4, 5], and the FDM utilized in this study. Comparing these two one realizes that the FEM approach yields better results. Due to the nature of FEM one can refine the mesh to obtain better results, something that cannot be done with FDM. Hence, we can conclude that the FEM approach is better than the FDM approach.

The implication of these findings suggest that while advanced regularization techniques can offer improvements, their practical application may be limited simply by parameter tuning. This highlights the importance of developing robust algorithms that require minimal manual intervention. One limitation of this study is the dependence on the initial guess for the reconstruction matrix, which can significantly impact the results. Future research could explore more sophisticated initialization methods or adaptive algorithms that reduce this dependency. Future studies could also investigate the integration of machine learning to automate the parameter selection process.

By addressing these points, we aim to make the application of hyperthermia more practical and reliable in real-world scenarios.

References

[1] Robert A. Adams and John Fournier. *Sobolev Spaces*. 2nd. Vol. 140. Pure and Applied Mathematics. Originally published in 1975. Boston, MA: Academic Press, 2003. ISBN: 9780120441433.

[2] H. Araki. *Mathematics: Concepts, and Foundations*. Encyclopedia of life support systems, mathematical sciences v. 2. Eolss Publishers Company Limited, 2009. ISBN: 9781848265806.

[3] Morteza Ghaderi Aram, Larisa Beilina, and Hana Dobsicek Trefna. "Microwave thermometry with potential application in non-invasive monitoring of hyperthermia". In: *Journal of Inverse and Ill-posed Problems* 28.5 (2020), pp. 739–750. DOI: doi:10.1515/jiip-2020-0102. URL: https://doi.org/10.1515/jiip-2020-0102.

[4] L. Beilina et al. "Truncated SVD for Applications in Microwave Thermometry". In: *Gas Dynamics with Applications in Industry and Life Sciences*. Ed. by Mohammad Asadzadeh, Larisa Beilina, and Shigeru Takata. Cham: Springer International Publishing, 2023, pp. 143–165. ISBN: 978-3-031-35871-5.

[5] Larisa Beilina, Morteza Ghaderi Aram, and Evgenii M. Karchevskii. "An adaptive finite element method for solving 3D electromagnetic volume integral equation with applications in microwave thermometry". In: *Journal of Computational Physics* 459 (2022), p. 111122. ISSN: 0021-9991. DOI: https://doi.org/10.1016/j.jcp.2022.111122. URL: https://www.sciencedirect.com/science/article/pii/S002199912200184X.

[6] Larisa Beilina, Evgenii Karchevskii, and Mikhail Karchevskii. *Numerical Linear Algebra: Theory and Applications*. English. Hardcover. Springer, Jan. 22, 2018. ISBN: 978-3319573021.

[7] Barkha Bindu, Ashish Bindra, and Girija Rath. "Temperature management under general anesthesia: Compulsion or option". In: *J. Anaesthesiol. Clin. Pharmacol.* 33.3 (July 2017), pp. 306–316.

[8] Peter Bloem. *Unraveling principal component analysis: A long-form guide through the mathematical fundamentals of data science and machine learning*. Independently published, July 2, 2023, p. 265. ISBN: 979-8850607159.

[9] R.R. Bowman. "A Probe for Measuring Temperature in Radio-Frequency-Heated Material (Short Papers)". In: *IEEE Transactions on Microwave Theory and Techniques* 24.1 (1976), pp. 43–45. DOI: 10.1109/TMTT.1976.1128763.

[10] D. Calvetti et al. “Tikhonov regularization and the L-curve for large discrete ill-posed problems”. In: *Journal of Computational and Applied Mathematics* 123.1 (2000). Numerical Analysis 2000. Vol. III: Linear Algebra, pp. 423–446. ISSN: 0377-0427. DOI: https://doi.org/10.1016/S0377-0427(00)00414-3. URL: https://www.sciencedirect.com/science/article/pii/S0377042700004143.

[11] Guanbo Chen et al. “Real-time three-dimensional microwave monitoring of interstitial thermal therapy”. In: *IEEE Trans. Biomed. Eng.* 65.3 (Mar. 2018), pp. 528–538.

[12] Kung-Shan Cheng et al. “Effective learning strategies for real-time image-guided adaptive control of multiple-source hyperthermia applicators”. In: *Med. Phys.* 37.3 (Mar. 2010), pp. 1285–1297.

[13] Weng Cho Chew. *Waves and Fields in Inhomogenous Media*. Paperback. Wiley-IEEE Press, Feb. 2, 1999. ISBN: 978-0780347496.

[14] David Colton and Rainer Kress. “Time harmonic electromagnetic waves in an inhomogeneous medium”. In: *Proceedings of the Royal Society of Edinburgh: Section A Mathematics* 116.3–4 (1990), pp. 279–293. DOI: 10.1017/S0308210500031516.

[15] N.R. Datta et al. “Local hyperthermia combined with radiotherapy and-/or chemotherapy: Recent advances and promises for the future”. In: *Cancer Treatment Reviews* 41.9 (2015), pp. 742–753. ISSN: 0305-7372. DOI: https://doi.org/10.1016/j.ctrv.2015.05.009. URL: https://www.sciencedirect.com/science/article/pii/S0305737215001048.

[16] Lawrence Craig Evans and Ronald F. Gariepy. *Measure Theory and Fine Properties of Functions, Revised Edition (Textbooks in Mathematics)*. Hardcover. Routledge, Apr. 20, 2015. ISBN: 978-1482242386.

[17] “Front Matter”. In: *An Introduction to the Finite Element Method for Differential Equations*. John Wiley Sons, Ltd, 2020. ISBN: 9781119671688. DOI: https://doi.org/10.1002/9781119671688.fmatter. eprint: https://onlinelibrary.wiley.com/doi/pdf/10.1002/9781119671688.fmatter. URL: https://onlinelibrary.wiley.com/doi/abs/10.1002/9781119671688.fmatter.

[18] Johanna Gellermann et al. “Noninvasive magnetic resonance thermography of soft tissue sarcomas during regional hyperthermia: correlation with response and direct thermometry”. In: *Cancer* 107.6 (Sept. 2006), pp. 1373–1382.

[19] C Groetsch. “The theory of Tikhonov regularization for Fredholm equations”. In: *104p, Boston Pitman Publication* (1984).

[20] Nail A Gumerov and Ramani Duraiswami. *Fast Multipole Methods for the Helmholtz Equation in Three Dimensions (Elsevier Series in Electromagnetism)*. Hardcover. Elsevier Science, Feb. 10, 2005. ISBN: 978-0080443713.

[21] Per Christian Hansen. “Analysis of Discrete Ill-Posed Problems by Means of the L-Curve”. In: *SIAM Review* 34.4 (1992), pp. 561–580. ISSN: 00361445. URL: http://www.jstor.org/stable/2132628 (visited on 05/21/2024).

[22] Per Christian Hansen. "REGULARIZATION TOOLS: A Matlab package for analysis and solution of discrete ill-posed problems". In: *Numerical Algorithms* 6.1 (Mar. 1994), pp. 1–35. ISSN: 1572-9265. DOI: 10.1007/BF02149761. URL: https://doi.org/10.1007/BF02149761.

[23] Mark Haynes, John Stang, and Mahta Moghaddam. "Real-time microwave imaging of differential temperature for thermal therapy monitoring". In: *IEEE Trans. Biomed. Eng.* 61.6 (June 2014), pp. 1787–1797.

[24] Kazufumi Ito and Bangti Jin. *Inverse problems: Tikhonov theory and algorithms*. Hardcover. World Scientific Publishing. ISBN: 978-9814596190.

[25] Peter R. Johnston and Ramesh M. Gulrajani. "An Analysis of the Zero-Crossing Method for Choosing Regularization Parameters". In: *SIAM Journal on Scientific Computing* 24.2 (2002), pp. 428–442. DOI: 10.1137/S1064827500373516. URL: https://doi.org/10.1137/S1064827500373516.

[26] A. Katzir et al. "Infrared fibers for radiometer thermometry in hypothermia and hyperthermia treatment". In: *IEEE Transactions on Biomedical Engineering* 36.6 (1989), pp. 634–637. DOI: 10.1109/10.29459.

[27] David C. Lay. *Linear Algebra and Its Applications, 4th Edition*. English. Hardcover. Pearson, Jan. 20, 2011. ISBN: 978-0321385178.

[28] *Matlab Code for choosing optimal regularization parameter*. URL: https://git.chalmers.se/alsaberi/regularized-algorithms-for-applications-in-microwave-thermometry-masters-project.

[29] Peter Monk. *Finite Element Methods for Maxwell's Equations (Numerical Mathematics and Scientific Computation)*. Hardcover. Clarendon Press, June 19, 2003. ISBN: 978-0198508885.

[30] et al. Nikola Cihoric. "Hyperthermia-related clinical trials on cancer treatment within the ClinicalTrials.gov registry". In: *International Journal of Hyperthermia* 31.6 (2015), pp. 609–614. DOI: 10.3109/02656736.2015.1040471. URL: https://doi.org/10.3109/02656736.2015.1040471.

[31] M. Roser and H. Ritchie. "Cancer". In: *Our World in Data* (2024). URL: https://ourworldindata.org/cancer.

[32] Elias M. Stein and Rami Shakarchi. *Introduction to Further Topics in Analysis*. Princeton: Princeton University Press, 2012. ISBN: 9781400840557. DOI: doi:10.1515/9781400840557. URL: https://doi.org/10.1515/9781400840557.

[33] Terence Tao. *An Introduction to Measure Theory (Graduate Studies in Mathematics, 126)*. Paperback. American Mathematical Society, Sept. 3, 2021, p. 206. ISBN: 978-1470466404.

[34] "What Is Cancer?" In: *National Cancer Institute* (2024). URL: www.cancer.gov/about-cancer/understanding/what-is-cancer.

[35] Lukas Winter et al. "Magnetic resonance thermometry: Methodology, pitfalls and practical solutions". In: *Int. J. Hyperthermia* 32.1 (2016), pp. 63–75.

[36] Gulsah Yildiz et al. “Comparison of Microwave Hyperthermia Applicator Designs with Fora Dipole and Connected Array”. In: *Sensors* 23.14 (2023). ISSN: 1424-8220. DOI: 10.3390/s23146592. URL: https://www.mdpi.com/1424-8220/23/14/6592.

[37] Daocheng Yu et al. “The Tikhonov-L-curve regularization method for determining the best geoid gradients from SWOT altimetry”. In: *Journal of Geodesy* 97.10 (Oct. 2023), p. 93. ISSN: 1432-1394. DOI: 10.1007/s00190-023-01783-5. URL: https://doi.org/10.1007/s00190-023-01783-5.

[38] Marcin Ziolkowski and Stanislaw Gratkowski. “Closed-Form Expressions for Local Absorbing Boundary Conditions in Electromagnetic Scattering Problems and Their Implementation into Commercial FEM Software”. In: *Energies* 17.1 (2024). ISSN: 1996-1073. DOI: 10.3390/en17010089. URL: https://www.mdpi.com/1996-1073/17/1/89.

DEPARTMENT OF MATHEMATICS
CHALMERS UNIVERSITY OF TECHNOLOGY
Gothenburg, Sweden
www.chalmers.se

CHALMERS
UNIVERSITY OF TECHNOLOGY